

1 **Title**

2 Phenotypic and functional characterisation of first trimester human placental macrophages,  
3 Hofbauer cells.

4

5 **One sentence summary**

6 Hofbauer cells are primitive placental macrophages with a unique phenotype and role in fetal  
7 defence.

8

9 **Authors**

10 Jake Thomas<sup>1,2</sup>, Anna Appios<sup>1,2</sup>, Xiaohui Zhao<sup>2</sup>, Roksana Dutkiewicz<sup>1</sup>, Maria Donde<sup>1</sup>, Colin  
11 Lee<sup>1</sup>, Praveena Naidu<sup>1,2</sup>, Christopher Lee<sup>3,4</sup>, Joana Cerveira<sup>1</sup>, Bing Liu<sup>5,6,7</sup>, Florent  
12 Ginhoux<sup>3,4,8,9</sup>, Graham Burton<sup>2</sup>, Russell S. Hamilton<sup>2,10</sup>, Ashley Moffett<sup>1,2</sup>, Andrew  
13 Sharkey<sup>1,2</sup>, Naomi McGovern<sup>1,2\*</sup>

14

15 **Affiliations**

- 16 1. Department of Pathology, University of Cambridge, Tennis Court Road, Cambridge,  
17 CB2 1QP, UK
- 18 2. Centre for Trophoblast Research, Department of Physiology, Development and  
19 Neuroscience, University of Cambridge, Cambridge, CB2 3DY, UK
- 20 3. Singapore Immunology Network (SIgN), Agency for Science, Technology and  
21 Research (A\*STAR), 8A Biomedical Grove, Immunos Building #3-4, Biopolis,  
22 Singapore 138648, Singapore
- 23 4. School of Biological Sciences, Nanyang Technological University, Singapore,  
24 Singapore.

- 25 5. Key Laboratory for Regenerative Medicine of Ministry of Education, Institute of  
26 Hematology, School of Medicine, Jinan University, Guangzhou, China.
- 27 6. State Key Laboratory of Proteomics, Academy of Military Medical Sciences,  
28 Academy of Military Sciences, Beijing, China
- 29 7. State Key Laboratory of Experimental Hematology, Institute of Hematology and  
30 Blood Diseases Hospital, Chinese Academy of Medical Sciences, Tianjin, 300020,  
31 China
- 32 8. Shanghai Institute of Immunology, Shanghai JiaoTong University School of Medicine,  
33 280 South Chongqing Road, Shanghai 200025, China
- 34 9. Translational Immunology Institute, SingHealth Duke-NUS Academic Medical  
35 Centre, 169856, Singapore
- 36 10. Department of Genetics, University of Cambridge, Downing Street, Cambridge, CB2  
37 3EH  
38

39 \*Correspondence: [nm390@cam.ac.uk](mailto:nm390@cam.ac.uk), [ORCID: 0001-5200-2698](https://orcid.org/0001-5200-2698)  
40

41

42

### 43 **Summary**

44 Using transcriptomic and proteomic data, Thomas, J. et al, analyse human first trimester  
45 placental macrophages and delineate markers that identify them. They also reveal that  
46 Hofbauer cells have microbicidal capacity, providing the fetus with an additional layer of  
47 protection from certain microbes.

48

### 49 **Abstract**

50 Hofbauer cells (HBC) are a population of macrophages found in high abundance  
51 within the stroma of the first trimester human placenta. HBC are the only fetal immune cell  
52 population within the stroma of healthy placenta. However, the functional properties of these

53 cells are poorly described. Aligning with their predicted origin via primitive haematopoiesis,  
54 we find that HBC are transcriptionally similar to yolk sac macrophages. Phenotypically, HBC  
55 can be identified as HLA-DR-FOLR2<sup>+</sup> macrophages. We identify a number of factors HBC  
56 secrete (including IL-8 and MMP-9) that could affect placental angiogenesis and  
57 remodelling. We determine that HBC have the capacity to play a defensive role, where they  
58 are responsive to Toll-like receptor stimulation and are microbicidal. Finally, we also identify  
59 a population of placenta-associated maternal macrophages (PAMM1a) that adhere to the  
60 placental surface and express factors, such as fibronectin, that may aid in repair.

61

## 62 **Non-standard abbreviation**

63 Placental associated maternal monocytes/macrophages, PAMM.

64

## 65 **Introduction**

66 Macrophages are found within all human tissues where, within the adult, they mediate  
67 tissue homeostasis, development, repair and immunity. During embryonic development the  
68 first macrophages to seed all tissues are derived through a process called primitive  
69 haematopoiesis. These macrophages, commonly termed ‘primitive’ macrophages, are distinct  
70 to those generated through definitive haematopoiesis as there is no monocyte  
71 intermediate (Ginhoux et al., 2010; Gomez Perdiguero et al., 2015). Although in some species  
72 such as the mouse, primitive haematopoiesis is thought to only occur within the yolk sac  
73 (YS), during human embryonic development primitive haematopoiesis also takes place in the  
74 placenta (Van Handel et al., 2010).

75 The placenta is a major organ that regulates the health of both the mother and  
76 developing fetus during pregnancy. The human placenta develops from the trophoctoderm,  
77 the outer layer of the pre-implantation blastocyst, which forms at ~5 days post fertilisation

78 (dpf)(Turco and Moffett, 2019). As the placenta develops, highly branched villous tree-like  
79 structures form, which contain fibroblasts, immature capillaries and macrophages, termed  
80 Hofbauer cells (HBC) (**Figure 1A**). The mesenchymal core is surrounded by a bilayer of  
81 specialized placental epithelial cells called trophoblast. The outermost syncytiotrophoblast  
82 (SCT) layer, in contact with maternal blood, is formed by fusion of underlying  
83 cytotrophoblast cells(Turco and Moffett, 2019). HBC have been identified within the  
84 placenta around day 18 post-conception(Castellucci et al., 1987; Boyd et al., 1970), before  
85 the placenta is connected to the embryonic circulation(Van Handel et al., 2010).

86 A number of recent studies have profiled the gene expression of human embryonic  
87 macrophage populations(Stewart et al., 2019; Vento-Tormo et al., 2018). However, studies  
88 demonstrating their functional properties remain limited. Our previous work demonstrating  
89 that 2<sup>nd</sup> trimester fetal dendritic cells are functionally active and responsive to TLR  
90 stimulation(McGovern et al., 2017) led us to query if primitive macrophages have similar  
91 capabilities. In particular, we were interested in determining if HBC demonstrate  
92 microbicidal capacity, as they are the only fetal immune cells found within the stroma of the  
93 human placenta, the crucial tissue barrier-site between maternal tissues and the fetus.

94 In this study we sought to develop a technique that would allow us to characterise the  
95 properties of HBC isolated from first trimester human placentas. Using a novel flow  
96 cytometric gating strategy, we find that commonly used protocols for the isolation of HBC  
97 from first trimester placentas yield a heterogenous population of macrophages that also  
98 consist of placenta-associated maternal monocyte/macrophage (PAMM) subsets. We  
99 demonstrate that HBC have a unique phenotype, specific to the placental niche; they do not  
100 express HLA-DR and highly express folate receptor 2 (FOLR2). We identify a range of  
101 factors HBC secrete that possibly affect placental angiogenesis and remodelling, including  
102 IL-8, osteopontin and MMP-9. We show that HBC are responsive to TLR stimulation and do

103 have microbicidal capacity, and can thereby play a defensive role for the fetus. Finally, we  
104 identify a novel population of placenta-associated maternal macrophages (PAMM1a), that  
105 could function in tissue repair. Our findings provide novel insights into the properties of  
106 human primitive macrophages, and the roles of HBC in placental homeostasis.

107

## 108 **Results**

### 109 **Identification of Hofbauer cells using anti-HLA antibodies**

110 Previous reports phenotyping HBC isolated from the placenta have yielded  
111 conflicting results(Sutton et al., 1983; Böckle et al., 2008; Bulmer et al., 1988; Goldstein et  
112 al., 1988; Reyes and Golos, 2018). We first sought to determine the true identity of first  
113 trimester HBC using multi-parameter flow cytometry. Employing a commonly used protocol  
114 to isolate HBC(Tang et al., 2011) (**Figure S1A**), we obtain a CD45<sup>+</sup>CD14<sup>+</sup> macrophage  
115 population that is heterogeneous for HLA-DR expression (**Figure 1B**). We sought to  
116 determine if the observed heterogeneity is due to maternal monocyte/macrophage populations  
117 contaminating the HBC placental isolates.

118 Fetal cells express both maternally and paternally derived genes. To determine if  
119 maternal cells contaminate the HBC preparations and contribute to the heterogeneity in  
120 observed HLA-DR expression, we added antibodies to common HLA allotypes (HLA-A3,  
121 HLA-B7 and HLA-A2) to our flow cytometry panel. The specificity of these antibodies was  
122 previously verified by quantitative polymerase chain reaction (qPCR) on DNA from blood  
123 samples of HLA-typed donors. We chose to use anti-HLA antibodies instead of sex  
124 chromatin staining (to identify male fetal cells), so that we could develop a flow cytometry  
125 panel to allow isolation of live cells for functional assays. By using anti-HLA antibodies and  
126 analysing matched maternal blood or decidual cells (**Figure S1D, S1E**), we consistently  
127 observe that the variable population of HLA-DR<sup>+</sup> cells in first trimester placental digests are

128 maternal in origin (**Figure 1C, S1A-C**). We termed the maternal cells obtained in placenta  
129 digests ‘placenta-associated maternal monocytes/macrophages’ (PAMM).

130 We had expected that maternal contamination of placental macrophage cell isolates  
131 would only become significant from the 10<sup>th</sup> week of gestation, the time when maternal blood  
132 flow to the intervillous space is fully established(Burton et al., 2009b). However, application  
133 of our new gating strategy to placental digests of 7-9 wk estimated gestational age (EGA) and  
134 10-12 wk EGA, demonstrated that maternal cells make a significant contribution to the  
135 CD14<sup>+</sup> macrophage populations isolated from the placenta as early as the 7<sup>th</sup> week of  
136 gestation, comprising 20-40% of CD14<sup>+</sup> cells (**Figure 1D**). Whole-mount  
137 immunofluorescence microscopy revealed that while HLA-DR<sup>+</sup> cells do adhere to the SCT  
138 layer of the placental villi, HLA-DR<sup>+</sup> cells are not present within the stromal core from the 7<sup>th</sup>  
139 to 10<sup>th</sup> week of gestation (**Figure 1E**). These findings are in line with recent single cell RNA  
140 sequencing (scRNAseq) studies of placental cell isolates(Tsang et al., 2017; Vento-Tormo et  
141 al., 2018) where maternal cells were also observed. Our data demonstrate that maternal cell  
142 contamination is higher than has previously been appreciated within first trimester placental  
143 cell suspensions. These findings will have a significant impact on *in vitro* studies that aim to  
144 determine the specific functional properties of HBC.

145

#### 146 **Identification of specific markers for HBC**

147 A limitation of using anti-HLA antibodies is that they can only distinguish maternal  
148 and fetal cells where there is a maternal/fetal HLA-mismatch for these specific allotypes. We  
149 therefore sought to identify markers that would allow us to confidently distinguish maternal  
150 from fetal cells independently of HLA antibodies. To do this, we carried out transcriptomic  
151 analysis of first trimester placental cells using a publicly available scRNAseq dataset(Vento-  
152 Tormo et al., 2018). Clustering and uniform manifold approximation and projection (UMAP)

153 visualisation of 22,618 placental single cells identifies 2 distinct macrophage populations, as  
154 indicated by *CD68* expression (**Figure S1F, S1G**). Consistent with our flow cytometry  
155 analysis, PAMM can be readily identified as HLA-DR<sup>hi</sup>, while HBC are HLA-DR<sup>-</sup> (**Figure**  
156 **S1G**). Expression of male (*RPS4Y1*) and female (*XIST*) specific genes in placental cells from  
157 male fetal donors confirms the fetal and maternal origin of HBC and PAMM clusters (**Figure**  
158 **S1H**).

159 A total of 962 genes are significantly differentially expressed genes (DEGs) (adjusted  
160 p value < 0.01) between PAMM and HBC clusters. *FCGR1A*, *FCGR1B*, *VSIG4*, *MRC1*,  
161 *FOLR2* and *LYVE-1* are upregulated within HBC. Unlike adult macrophages, HBC do not  
162 express HLA-DR. In contrast, PAMM highly express *HLA-DRB1* and *HLA-DRA* (**Figure**  
163 **1F**). We tested a number of additional HBC specific markers that were identified by analysis  
164 of the sequencing data, including FOLR2, CD64 and CD206. We also analysed the  
165 expression of arginase 2, which has previously been shown to be expressed by fetal immune  
166 cells (McGovern et al., 2017). Samples from donors where the anti-HLA antibodies  
167 distinguished maternal from fetal cells were used. These markers are expressed by HBC at  
168 the protein level by flow cytometry (**Figure 1G**). Any of these 4 markers, in combination  
169 with HLA-DR, allows us to confidently distinguish HBC from PAMM within first trimester  
170 samples. The combination of FOLR2 and HLA-DR provides the clearest separation for the  
171 isolation of HBC.

172

### 173 **Hofbauer cells are transcriptionally similar to ‘primitive’ macrophages and proliferate** 174 ***in situ***

175 HBC are predicted to be ‘primitive’ macrophages derived directly from progenitors  
176 independent of monocytes. A recent study characterising the transcriptional landscape of  
177 human macrophage development, identified a population of true primitive yolk sac

178 macrophages (YS\_Mac1) from a Carnegie stage 11 embryo (~4 weeks post conception)(Bian  
179 et al., 2020). Consistent with their predicted primitive origins, HBC are enriched for a gene  
180 signature derived from YS\_Mac1, but not embryonic monocytes (**Figure 2A,**  
181 **Supplementary File 1**). Integration of first trimester placental(Vento-Tormo et al., 2018) and  
182 early human fetal myeloid scRNAseq(Bian et al., 2020) datasets reveals a high degree of  
183 transcriptional similarity between HBC and primitive YS\_Mac1 (**Figure 2B, 2C**). PAMM  
184 however, display transcriptional similarity to embryonic monocytes, reflecting their  
185 monocytic origins (**Figure 2A, 2C**).

186 HBC are also highly enriched for a gene signature from YS-derived embryonic  
187 macrophages from a Carnegie stage 10 embryo (~4 weeks post conception) (CS10 mac) from  
188 an additional dataset(Zeng et al., 2019) (**Figure 2D, Supplementary File 1**). PAMM display  
189 intermediate levels of enrichment for the CS10 mac gene signature. This is likely due to  
190 conserved myeloid genes not specific to ‘primitive’ macrophages within the gene signature,  
191 as it was generated via comparison between CS10 macs and non-immune cells in that dataset  
192 (**Materials and Methods**). Analysis of individual genes reveals further similarity between  
193 HBC, YS\_Mac1 and CS10 mac, on the basis of *HLA-DRB1* and *FOLR2* expression (**Figure**  
194 **2E**).

195 Due to the transcriptional similarity between HBC and ‘primitive’ macrophages, we  
196 hypothesised that HBC would be maintained in the tissue via local proliferation. We find that  
197 ~11% of freshly isolated HBC express Ki67 by flow cytometry (**Figure 2F, S1I**) and identify  
198 Ki67<sup>+</sup> cells within the stroma of placental villi by immunohistochemistry (IHC) (**Figure 2G**).  
199 Furthermore, during overnight culture, ~1.5% of FACS-isolated HBC incorporate 5-Ethynyl-  
200 2'-deoxyuridine (EDU), and incorporation is slightly elevated by the addition of macrophage  
201 colony-stimulating factor (MCSF) to the cultures (**Figure 2H**). Directed analysis of the HBC  
202 cluster within the placental scRNAseq dataset identifies 2 proliferating populations, pHBC-1



203 and pHBC-2 (**Figure 2I**). These clusters express genes associated with distinct stages of the  
204 cell cycle (*PTTG1*, *CDC20*, *UBE2C*, *CDK1*, *PCNA* and *MCM5*) (**Figure 2J**), and cell cycle  
205 scoring assigns pHBC-1 and pHBC-2 to the S and G2/M phases of the cell cycle respectively  
206 (**Figure 2K**). RNA velocity vectors, derived by calculating the ratio between spliced and  
207 unspliced reads of each gene within each cell (La Manno et al., 2018), demonstrate a clear  
208 path of HBC through the cell cycle (**Figure 2K**). No subpopulations are observed within non-  
209 proliferating HBC, allowing us to isolate them as a single population for functional assays.

210 Together these data show that HBC are transcriptionally similar to macrophage  
211 populations generated through primitive haematopoiesis and are a homogenous population,  
212 proliferating within placental villi, suggesting that they arise without a monocyte  
213 intermediate.

214

### 215 **PAMM are heterogeneous**

216 Our flow cytometric analysis clearly shows that PAMM consist of 2 major  
217 populations, HLA-DR<sup>hi/lo</sup>FOLR2<sup>-</sup> cells (PAMM1) and HLA-DR<sup>hi</sup>FOLR2<sup>hi</sup> cells (PAMM2)  
218 (**Figure 3A**). Subsequently, directed reanalysis of PAMM within the scRNAseq dataset  
219 reveals further heterogeneity on the basis of *CD9*, but not *FOLR2* expression (**Figure 3B**).  
220 Adding CD9 to our flow cytometry panel, the HLA-DR<sup>hi/lo</sup>FOLR2<sup>-</sup> (PAMM1) cells are split  
221 into two populations (**Figure 3C**). To determine if either of these populations are circulating  
222 maternal monocytes, we added the monocyte marker *CCR2* to the panel and performed flow  
223 cytometry on matched maternal blood. FOLR2<sup>-</sup>CD9<sup>hi</sup>CCR2<sup>lo/int</sup> cells are not present in  
224 matched maternal blood, indicating that they are macrophages with a phenotype specific to  
225 the placental niche. The remaining PAMM1 cells do however share a similar phenotype with  
226 maternal peripheral blood monocytes (**Figure 3D**). Therefore, we subdivided PAMM1 into  
227 two populations: PAMM1a, FOLR2<sup>-</sup>CD9<sup>hi</sup>CCR2<sup>lo/int</sup> (macrophages), and PAMM1b, FOLR2<sup>-</sup>

228 CD9<sup>-int</sup>CCR2<sup>+</sup> (monocytes) (**Figure 3E, S1J**).

229 HLA-DR<sup>hi</sup>FOLR2<sup>hi</sup> cells (PAMM2) are rare in placental samples (~3% of placental

230 CD14<sup>+</sup> cells) (**Figure 3F**). Decidual macrophages also express FOLR2 and HLA-DR (**Figure**

231 **S2A, S2B**) and it is likely that PAMM2 are maternal decidual macrophages that will

232 contaminate placental samples. Although PAMM2 do not form a distinct cluster in the

233 placental scRNAseq dataset, combined analysis of placental, decidual and maternal blood

234 scRNAseq datasets (**Figure S2C**) reveals that HLA-DR<sup>+</sup> FOLR2<sup>+</sup> decidual macrophages

235 (dMac2) (**Figure S2D**) are found in low numbers in the placental digests (**Figure**

236 **S2E**)(Vento-Tormo et al., 2018). Cytospins and analysis of cell granularity and size by flow

237 cytometry shows that HBC, PAMM1a and PAMM2 are large, granular cells with

238 morphologies typical of macrophages - large vacuoles and pseudopods (**Figure 3G, 3H, 3I**).

239 PAMM1b are comparatively smaller in size, and their morphology is typical of blood

240 monocytes (**Figure 3G, 3H, 3I**). In line with their phenotypic and morphological properties,

241 we find that PAMM1b are transcriptionally similar to adult circulating classical monocytes

242 (**Figure S2F**). However, PAMM1b display increased expression of 150 genes, including

243 chemokines, in comparison to maternal blood classical monocytes (**Figure S2G**). PAMM1a

244 are not present within the decidua (**Figure S2A**), indicating their phenotype probably reflects

245 adherence to the SCT. Of the three PAMM populations identified, PAMM1a are the most

246 abundant, representing ~11% of the CD14<sup>+</sup> cells in placental isolates (**Figure 3F**).

247 In conclusion PAMM can be subdivided into different populations. PAMM1b are

248 monocytes, PAMM1a are macrophages that are specific to the placental surface, whilst

249 PAMM2 are contaminating decidual macrophages.

250

251 **PAMM1a adhere to sites of injury on the placental surface and secrete factors involved**

252 **in tissue repair**

253 We next sought to determine the potential role of PAMM1a in healthy pregnancy. To  
254 investigate what changes in gene expression occur during the transition from PAMM1b  
255 (monocytes) to PAMM1a (macrophages) we performed Slingshot trajectory analysis(Street et  
256 al., 2018) (**Figure 4A**). Genes associated with monocyte identity and function, including  
257 *S100A8*, *S100A9* and *LYZ*, are downregulated along the trajectory (**Figure 4B**). Upregulated  
258 genes included macrophage markers *CD63*, *CD68*, *CD36* and *GPNMB*, and a subset of genes  
259 associated with tissue remodelling (including *LPL*, *MMP7*, and *MMP9*) (**Figure 4C**). The  
260 elevated surface expression of LOX-1 (the receptor encoded by *OLR1*), *CD63*, *CD68* and  
261 *CD36* by PAMM1a are verified by flow cytometry (**Figure 4D**).

262 Breaks occur in the SCT *in vivo* in healthy pregnancies(Burton and Watson, 1997).  
263 Fibrin deposits together with macrophages are characteristically seen at the sites of syncytial  
264 damage(Pierleoni et al., 2003; Burton and Watson, 1997). We identify PAMM1a adhered to  
265 sites of damage on the SCT by electron (**Figure 4E, S2H**) and fluorescent microscopy  
266 (**Figure 4F**). PAMM1a secrete matrix metalloproteinase (MMP)-9 (detected by Luminex  
267 assay after FACS isolation and overnight culture) (**Figure 4G**) and strongly express  
268 fibronectin (mRNA) (**Figure 4H**). Transmission electron microscopy reveals PAMM1a are  
269 laden with lipid droplet-like structures (yellow arrows **Figure 4E**). Staining with BODIPY, a  
270 dye that specifically labels neutral lipids, confirms that PAMM1a are highly loaded with lipid  
271 droplets (**Figure 4I, S2I, S2J**). Lipid droplet formation in macrophages can be induced by the  
272 uptake of apoptotic cells(Ward et al., 2018; Ford et al., 2019; D'Avila et al., 2011),  
273 suggesting PAMM1a function in the clearance of cellular debris and repair of the SCT  
274 following damage. If this is the case, PAMM1a might display transcriptomic similarities to  
275 macrophages in damaged, fibrotic tissues. Indeed, we find that PAMM1a, but not HBC, are  
276 strongly enriched for a gene signature from a population of scar-associated macrophages

277 found in human cirrhotic livers(Ramachandran et al., 2019)(**Figure 4J, Supplementary File**  
278 **1**).

279 To summarise, we have identified PAMM1a on the SCT, and these cells are likely to  
280 function in essential repair of the placental barrier.

281

### 282 **Hofbauer cells produce factors that promote placental angiogenesis**

283 HBC, PAMM1a and PAMM1b populations were isolated by FACS from placental  
284 digests, cultured overnight and their secretion of cytokines and growth factors was  
285 determined by Luminex (PAMM2 cell yields were too low for functional assays) (**Figure 5A,**  
286 **S3A**). The secretion profile of PAMM1a and PAMM1b differs substantially from HBC  
287 reflecting their maternal origin. PAMM1b secrete increased amounts of the proinflammatory  
288 cytokines IL-1 $\beta$  and IL-6 in comparison with PAMM1a (**Figure 5A**), consistent with a  
289 monocyte to macrophage transition. In comparison with PAMM1a and PAMM1b, HBC  
290 secrete both VEGF-A and low levels of FGF2, growth factors involved in placental growth  
291 and angiogenesis(Burton et al., 2009a; Arany and Hill, 1998) as well as high levels of  
292 osteopontin (OPN), that has a role in implantation and placentation(Johnson et al., 2003).  
293 Surprisingly, HBC also secrete factors that are typically associated with inflammation such as  
294 IL-8, CCL-2, 3 and 4. However, these factors also have pro-angiogenic properties, a more  
295 likely role in the context of the placenta(Shi and Wei, 2016; Lien et al., 2018; Wu et al.,  
296 2008; Salcedo et al., 2000; Stamatovic et al., 2006). HBC expressed tissue inhibitor of  
297 metalloproteinase (TIMP)-1 and MMP-9, both of which are involved in remodelling of  
298 placental vessels(Luizon et al., 2014; Plaks et al., 2013).

299 To determine which cells respond to factors secreted by HBC, we generated a  
300 measure of the interaction potential between HBC and other placental cells by combining  
301 Luminex protein secretion data with scRNAseq gene expression data for cognate receptors

302 **(Figure 5B)**. Our analysis reveals predicted targets of HBC signalling **(Figure 5C, S3B)**.  
303 Endothelial cells are the main target of VEGF-A secretion, mediated by the expression of  
304 kinase insert domain receptor (KDR) and neuropilin 1 (NRP1). OPN is also predicted to  
305 signal to endothelial cells, via CD44 and integrin complexes, interactions which are known to  
306 promote angiogenesis(Dai et al., 2009; Poggio et al., 2011). HBC-endothelial cell interactions  
307 are also facilitated by their close proximity within placental villi **(Figure S3C)**. Additionally,  
308 HBC are predicted to signal to placental fibroblasts via IL-6, and to villous cytotrophoblast  
309 via both OPN and granulocyte-macrophage colony-stimulating factor (GM-CSF).

310 In summary, we have identified factors that HBC secrete that are likely to promote  
311 placental growth and homeostasis through interactions with endothelial cells, fibroblasts and  
312 trophoblast.

313

#### 314 **Hofbauer cells are responsive to TLR stimulation**

315 The placenta is a crucial barrier protecting the fetus from vertical infections, and HBC  
316 are the only fetal myeloid cells in the first trimester placenta. However, their role in  
317 defending the fetus from infection remains unclear. In addition, whether ‘primitive’  
318 macrophages have the capacity to detect and respond to microbial stimuli is unknown. We  
319 therefore next asked whether HBC are responsive to Toll-like receptor (TLR) stimulation.  
320 TLRs drive specific immune responses through the recognition of distinct pathogen-  
321 associated molecular patterns, derived from a range of microbes(Kawasaki and Kawai, 2014).

322 The TLR expression profile of HBC analysed by flow cytometry is distinct from  
323 PAMM populations **(Figure 5D, S3D)**; while HBC express TLR2, 3, 4, 7 and 8, their  
324 expression of TLR-6 is elevated in comparison with PAMM1a and 1b. TLR9 expression is  
325 low to negative in HBC, PAMM1a and PAMM1b. Interestingly, TLR expression is poorly

326 captured by scRNAseq (**Figure S3E**), highlighting potential issues with over-reliance on  
327 gene expression data alone.

328 We next determined the response of HBC, PAMM1a and PAMM1b to TLR  
329 stimulation by analysing their production of cytokines and growth factors after overnight  
330 stimulation with TLR agonists. Due to differences between subsets in their baseline  
331 expression of cytokines and growth factors, as demonstrated in **Figure 5A**, expression levels  
332 are normalised to unstimulated controls (**Figure 5E, S4**). The response of HBC to TLR  
333 stimulation is specific to the agonist used, with LPS+IFN $\gamma$  and FSL-1, a TLR 6 agonist,  
334 having the greatest impact. A combination of LPS and IFN $\gamma$  impairs the ability of HBC to  
335 produce factors important in tissue remodelling, including TIMP-1 and MMP-9, and  
336 increases the secretion of IL-1 $\beta$  and TNF $\alpha$ . FSL-1 increases HBC production of CCL3, IL-8,  
337 IL-6 and GM-CSF. In contrast, PAMM1a and PAMM1b did not respond to FSL-1. These  
338 data show that ‘primitive’ HBC are capable of recognising and responding to microbial  
339 stimulation and highlight the distinct responses of HBC compared to maternal PAMM1a and  
340 PAMM1b.

341

#### 342 **Hofbauer cells demonstrate microbicidal capacity**

343 Given that breaks in SCT could provide a placental entry point for microbes and HBC  
344 are responsive to TLR stimulation, we next sought to determine if HBC have the mechanisms  
345 in place to kill microbes. Although mechanisms utilised by adult macrophages to kill  
346 microbes are well described in the literature, it remains unclear if ‘primitive’ macrophages  
347 such as HBC can utilise these.

348 HBC highly express receptors involved in phagocytosis, including CD64 (binds to  
349 IgG immune complexes), the mannose receptor CD206 (**Figure 1G**), and the scavenger  
350 receptors CD163, AXL and TIM1 (recognises phosphatidylserine (PS) and is critical for the

351 uptake of apoptotic cells(Kobayashi et al., 2007))(Figure S5A). In line with these findings  
352 HBC display increased phagocytic capacity of YG beads (Figure 6A) and CFSE-labelled  
353 *Escherichia coli* (Figure S5B) in comparison with PAMM1a. Cells cultured at 4°C and in the  
354 presence of cytochalasin D (an inhibitor of actin polymerisation) were used as controls for  
355 beads bound to the cellular surface.

356 During phagocytosis phagosomes fuse with lysosomes, resulting in production of  
357 reactive oxygen species (ROS) and protease activation. We tested if HBC can produce ROS  
358 using the ROS indicator CM-H2DCFDA. Isolated HBC make ROS even without phorbol 12-  
359 myristate 13-acetate (PMA) stimulation (Figure S5C), possibly due to the stress of the cell  
360 isolation protocol. Using *ex-vivo* whole-mount immunofluorescence microscopy on placental  
361 explants, we find that the CD64<sup>+</sup> HBC in the villous stroma produce ROS, indicated by CM-  
362 H2DCFCA staining (Figure 6B).

363 Both HBC and PAMM also express high levels of the protease cathepsin B (Figure  
364 6C). Cathepsin B is active within HBC and PAMM1a, as demonstrated using cathepsin  
365 Magic Red™ (Figure 6D, Figure S5D). HBC and PAMM1a also contain lysosomal  
366 structures that were identified by the addition of acridine orange (AO) (Figure 6E, Figure  
367 S5D). An acidic environment in phagosomes directly aids in bacterial killing and is also  
368 important for the activation of pH-sensitive antimicrobial enzymes(Sedlyarov et al., 2018;  
369 Flannagan et al., 2015). To determine if the HBC phagosome becomes acidic during  
370 maturation, we profiled the uptake of zymosan particles tagged with a pH sensitive probe  
371 (Carboxy SNARF ®-1)(Foote et al., 2017, 2019). After allowing phagocytosis for 20  
372 minutes, we find that the HBC phagosome becomes rapidly acidic, reaching a pH of  
373 ~4.5(Figure 6F, 6G). In contrast, the phagosomes of PAMM1a are more alkaline, with a pH  
374 of ~7.4 (Figure 6F, 6G). The pH of the PAMM1a phagosome is characteristic of antigen-  
375 presenting cells that are processing peptides for presentation(Savina et al., 2006).

376 Finally, to confirm that first trimester HBC have microbicidal capacity we cultured  
377 HBC with *Lactobacillus crispatus* (a microbe reported to be found in very low abundance  
378 within the 2<sup>nd</sup> trimester fetal intestine (Rackaityte et al., 2020)) and *Escherichia coli* (not  
379 found in the fetus(Rackaityte et al., 2020)). We find that HBC are as efficient as PAMM1a at  
380 killing both *L. crispatus* and *E. coli*, when cultured at a MOI of 1 (**Figure 6H, 6I**) and 10  
381 (**Figure S5E, S5F**).

382 Together, these data demonstrate that HBC, a population of ‘primitive’ macrophages,  
383 exhibit a range of microbicidal tools and have the capacity to kill bacteria *in vitro*.

384

## 385 **Discussion**

386 Here we describe methods for the identification, isolation and characterisation of first  
387 trimester HBC. We have summarised our key findings and conclusions in **Figure 6J**.  
388 Through the application of multi-parameter flow cytometry, anti-HLA antibodies and  
389 analysis of publicly available scRNAseq datasets, we find that CD14<sup>+</sup> cells obtained from  
390 first trimester placental digests contain both fetal macrophages and maternal  
391 monocytes/macrophages. Our results indicate that all previous findings on HBC from  
392 placental digests will include these maternal myeloid cells. PAMM constitute ~20-40% of  
393 isolated CD14<sup>+</sup> cells and consist of 3 populations, PAMM1a, PAMM1b and PAMM2.  
394 PAMM1a are maternal monocyte-derived macrophages that have adopted a phenotype  
395 specific to the placental niche. PAMM1b are very similar to maternal monocytes, but display  
396 elevated expression of 150 genes when compared to matched maternal blood monocytes.  
397 This may reflect an adaptation to their location in the intervillous space, a unique  
398 microenvironment which can attract specific immune cells during gestation(Solders et al.,  
399 2019). However, these differences in gene expression could also reflect the isolation process  
400 for placental cells. Given their similar phenotype, PAMM2 are likely to be decidual



401 macrophages, previously termed dMac2(Vento-Tormo et al., 2018), that contaminate the cell  
402 isolates from uterine/placental tissues from early pregnancy. They are relatively rare cells and  
403 their properties were not studied further.

404 Our data demonstrates that HBC are a homogenous population that are  
405 transcriptionally similar to primitive YS macrophages, further emphasising their origin  
406 through primitive haematopoiesis. While fate mapping studies using murine models have  
407 determined the origins of many tissue macrophage populations(Ginhoux and Guilliams,  
408 2016), the origin of HBC has yet to be elucidated. The placenta is a known site of primitive  
409 haematopoiesis(Van Handel et al., 2010), but whether it occurs independently of the yolk sac  
410 or if yolk sac macrophages migrate to the placenta giving rise to HBC is unknown. HBC, YS  
411 macrophages and YS-derived macrophages from a Carnegie stage 10 embryo do not express  
412 HLA-DR. This suggests that the lack of HLA-DR is an intrinsic property of primitive  
413 macrophages, and could be used to distinguish macrophages derived from primitive and  
414 definitive haematopoiesis in other fetal tissues.

415 Previous studies have yielded variable findings concerning the phenotype, cytokine  
416 secretion and functions of HBC(Johnson and Chakraborty, 2012; Young et al., 2015; Pavlov  
417 et al., 2020; Loegl et al., 2016; Schlieffsteiner et al., 2017; Swieboda et al., 2020), probably  
418 due to the failure to account for PAMM contamination which we show is present in placental  
419 digests. Here, using our gating strategy for the isolation of placental myeloid cell populations  
420 we find that steady-state HBC secrete a range of factors that play a role in vascularisation and  
421 the remodelling of blood vessels, such as VEGF-A, OPN, MMP-9 and TIMP-1(Johnson et  
422 al., 2003; Dai et al., 2009; Poggio et al., 2011; Luizon et al., 2014; Plaks et al., 2013). HBC  
423 also secrete factors that are typically associated with inflammation, including IL-8, CCL-2,  
424 CCL-3 and CCL-4. IL-8 is a potent neutrophil chemoattractant(Hammond et al., 1995) but  
425 neutrophils are absent from the healthy placenta. In the context of the placenta, it is therefore

426 likely that these factors are pro-angiogenic. For example, *in vitro* assays(Shi and Wei, 2016),  
427 using a physiological range of IL-8 (0.2 – 1 ng ml<sup>-1</sup>) (we found HBC produce ~128 ng ml<sup>-1</sup>  
428 <sup>1/10<sup>4</sup></sup> cells of IL-8), have shown that IL-8 promotes the migration and canalization of human  
429 umbilical vein endothelial cells (HUVECs) and their production of VEGF-A(Shi and Wei,  
430 2016).

431         The SCT layer that covers the placental surface always contains sites of damage  
432 during healthy pregnancy(Costa et al., 2017; Burton and Watson, 1997), particularly seen at  
433 bridges between 2 villi(Burton and Watson, 1997). Fibrin deposits are typically present at the  
434 sites of breaks in the syncytium(Burton and Watson, 1997). We suggest that PAMM1a are  
435 the macrophages that have been identified at sites of damage at the syncytium(Burton and  
436 Watson, 1997) and are mediators of the repair process, as they adopt a tissue-repair  
437 phenotype, and are transcriptionally similar to scar-associated macrophages in human liver  
438 fibrosis. PAMM1a are also laden with lipid droplets and are deficient in phagocytosis. This  
439 finding is resonant with data showing microglia laden with lipid droplets also display  
440 impaired phagocytosis(Marschallinger et al., 2020), although the responsible mechanisms are  
441 still unknown. PAMM1a may have reached a point of ‘saturation’ through the uptake of  
442 cellular debris at the placental surface, reducing further phagocytosis. In future studies, it will  
443 be interesting to determine the role of PAMM1a in pregnancy disorders including  
444 preeclampsia and transplacental infection.

445         Our work shows that while HBC are ‘primitive’ macrophages in terms of origin, they  
446 are not primitive in function, demonstrated by their response to TLR stimulation and their  
447 microbicidal capacity. The distinct response of HBC to TLR stimulation in comparison with  
448 PAMM1a reflects their TLR expression profile. For example, HBC highly express TLR-6  
449 (binds to bacterial lipoproteins) and strongly respond to TLR-6 stimulation in comparison  
450 with PAMM1a. The elevated expression of TLR-6 by HBC is surprising given its expression

451 is restricted to a select number of human tissues, such as the spleen(Fagerberg et al., 2014).  
452 While HBC demonstrate increased phagocytic capacity and adopt a more acidic phagosome  
453 in comparison with PAMM1a, PAMM1a are as efficient as HBC at killing both *E. coli* and *L.*  
454 *crispatus*. This equivalent microbicidal capacity can be explained by active cathepsin B  
455 activity and other anti-microbial mechanisms that PAMM1a may have. Given the  
456 microbicidal capacity of HBC, it is of interest to study their interaction with microbes that do  
457 cross the placental barrier and cause an adverse pregnancy outcome, such as *Listeria*  
458 *monocytogenes* and Zika virus. However, these areas of research were beyond the scope of  
459 this study.

460         The work presented in this study is limited to first trimester samples. Previous studies  
461 have investigated the properties of HBC across gestation(Goldstein et al., 1988; Ingman et  
462 al., 2010; Swieboda et al., 2020; Pavlov et al., 2020). However, studies that used placental  
463 digests have not considered contamination with PAMM populations and so interpretation of  
464 some of their findings is difficult. Using the methods described here for the isolation and  
465 study of HBC, an area of interesting future research will be to investigate how HBC  
466 phenotype and functions change throughout pregnancy.

467         In summary, we have provided a gating strategy that allows the study of human HBC.  
468 We have inferred the roles of these cells at the steady state and demonstrated the microbicidal  
469 capacity of human ‘primitive’ macrophages. This study adds to our understanding of human  
470 developmental immunology and provides an important framework for the field of placental  
471 biology. Future studies will now aim to determine the roles of ‘primitive’ HBC in health and  
472 disease.

473

## 474 **Methods and Materials**

### 475 **Patient samples**

476 All tissue samples used were obtained with written consent from participants.

477 Decidual and placental tissues were obtained from healthy women with apparently normal  
478 pregnancies undergoing elective first trimester terminations (6-12 weeks EGA) (n=20).

479 Peripheral blood was taken from women undergoing elective first trimester terminations (6–  
480 12 EGA). The EGA of the samples was determined from the last menstrual period. All  
481 samples were obtained with written informed consent from participants under ethical  
482 approval which was obtained from the Cambridge Research Ethics committee (study  
483 04/Q0108/23).

484

### 485 **Tissue processing**

486 Placental samples were processed immediately upon receipt. Samples were washed in  
487 PBS for 10 minutes with a stirrer before processing. The placental villi were scraped from the  
488 chorionic membrane with a scalpel and digested with 0.2% Trypsin (Pan-Biotech)/0.02%  
489 Ethylenediaminetetraacetic acid (EDTA) (Source BioScience) at 37°C with stirring, for 7  
490 minutes. The digested cell suspension was passed through a sterile muslin gauze, and fetal  
491 bovine serum (FBS) (Sigma-aldrich) was added to halt the digestion process. The undigested  
492 tissue left on the gauze was scraped off with a scalpel and digested in 2.5ml 1mg/ml  
493 collagenase V (Sigma-Aldrich), supplemented with 50ul of 10mg/ml DNase I (Roche) for 20  
494 minutes at 37°C with agitation. The digested cell suspension was passed through a sterile  
495 muslin gauze and washed through with PBS. Cell suspensions from both the trypsin and  
496 collagenase digests were pelleted, resuspended in PBS and combined. Cells were layered  
497 onto a Pancoll gradient (PAN-biotech) and spun for 20 minutes without brake at 3000

498 rotations per minute (rpm). The leukocyte layer was collected and washed in PBS. Decidual  
499 samples and blood were processed as described previously(Huhn et al., 2020).

500

### 501 **Flow cytometry**

502 Cell suspensions were stained for viability with either 1:3000 4',6-diamidino-2-  
503 phenylindole (DAPI) (Sigma-Aldrich) or 1:1000 Zombie Aqua (Biolegend) for 20 minutes at  
504 4°C, and washed twice in PBS. Cells were blocked in human blocking buffer (5% human  
505 serum (Sigma-Aldrich), 1% rat serum (Sigma-Aldrich), 1% mouse serum (Sigma-Aldrich),  
506 5% FBS and 2mM EDTA) for 15 minutes at 4°C, and were incubated with antibody cocktails  
507 for 30 minutes at 4°C. Antibodies used are listed in **Supplementary Table 1**. Cells were  
508 washed and resuspended in FACS buffer (PBS containing 2% FBS and 2mM EDTA). For  
509 intracellular staining, cells were fixed and permeabilised with BD Pharmingen™  
510 Transcription Factor Buffer (BD bioscience), according to manufacturer's instructions. The  
511 lineage (lin) channel in flow cytometry analyses included the markers CD3, CD19, CD20,  
512 CD66b and CD335, for the removal of contaminating maternal T cells, B cells, NK cells and  
513 granulocytes. Flow cytometry was performed using a Cytex Aurora (Cytex), or cells were  
514 purified by cell-sorting using a BD FACS Aria III (BD bioscience). All flow cytometry data  
515 was analysed using FlowJo v10.6.1 (Treestar).

516

### 517 **Whole mount immunofluorescence microscopy**

518 Biopsies of placental tissue (2 cm<sup>3</sup>) were prepared as described previously(Wang et  
519 al., 2014). Placental villi were blocked with microscopy blocking solution (1% BSA (Sigma-  
520 Aldrich), 0.25% Triton X-100 (Sigma-Aldrich) in PBS) for 15 minutes and stained with  
521 antibodies (**Supplementary Table 1**) suspended in microscopy blocking solution in 1.5ml  
522 Eppendorf tubes for 1 hour at room temperature or overnight at 4°C. The nuclear dye

523 Hoechst 33342 (Abcam) (diluted 1:2000 in PBS) was added for 30 minutes before imaging.

524 Whole mounts were mounted in a chamber system (POC-R2 cell cultivation system from

525 Pecon). Imaging was performed using a Zeiss SP8 confocal LSM 700.

526

## 527 **Electron Microscopy**

528 Correlative scanning and transmission electron microscopy images of PAMM on the

529 surface of first trimester placental villi were generated as previously described(Burton, 1986).

530

## 531 **Immunofluorescence of placental tissue sections**

532 First trimester placenta villous tissue and decidual sections were prepared as

533 described previously. Slides were placed in blocking buffer for 20 minutes at room

534 temperature, washed in PBS and incubated overnight at 4°C with antibodies (**Supplementary**

535 **Table 1**). The slides were washed twice for 5 minutes in PBS, and when necessary, incubated

536 with secondary antibodies for 1h at room temperature and washed twice for 5 minutes in

537 PBS. The slides were then air-dried and mounted using VECTASHIELD® Antifade

538 Mounting Medium with DAPI (Vector Laboratories). Slides were imaged using a Zeiss SP8

539 confocal LSM 700 (Zeiss).

540

## 541 **Immunohistochemistry**

542 Slides were prepared as described previously(Sharkey et al., 1999). Antibodies used

543 are indicated in **Supplementary Table 1**. Slides were imaged on an EVOS M5000

544 microscope (Thermo Fisher Scientific).

545

## 546 **BODIPY staining of placental cells**

547 Placental cells were stained for flow cytometry as described above. Cells were  
548 incubated in 2ng/ml BODIPY 493/503 (Thermo Fisher Scientific) in PBS for 20 minutes at  
549 4°C. Cells were washed in FACS buffer and acquired on a Cytex Aurora (Cytex).

550 FACS-isolated PAMM1a and PAMM1b were incubated in 250ng/ml BODIPY  
551 493/503 (Thermo Fisher Scientific) in PBS for 1 hour at 37°C, fixed in 4% paraformaldehyde  
552 solution (Sigma) and washed twice in PBS. Cytospins were prepared and mounted using  
553 VECTASHIELD® Antifade Mounting Medium with DAPI (Vector Laboratories) and imaged  
554 using a Zeiss SP8 confocal LSM 700.

555

#### 556 **5-Ethynyl-2'-deoxyuridine (EDU) incorporation assay**

557 FACS-purified HBC were plated at a density of 10,000 cells in 100ul of Dulbecco's  
558 Modified Eagle Medium (DMEM)(Thermo Fisher Scientific) supplemented with 10% FBS,  
559 2.5% Penicillin Streptomycin (Sigma-Aldrich) and 20µM L-Glutamine (Sigma-Aldrich).  
560 EDU incorporation was determined using the Click-IT™ Plus EdU Alexa Fluor™ 647 Flow  
561 Cytometry Assay Kit (Thermo Fisher Scientific), according to manufacturer's instructions.  
562 Cells were incubated for 18 hours prior to harvesting and acquisition by flow cytometry.

563

#### 564 **Cytokine production and Toll-like receptor stimulations**

565 FACS-purified HBC, PAMM1a and PAMM1b were plated into V-bottom 96 well  
566 plates at a density of 10,000 cells in 50µl of DMEM supplemented with 10% FBS, 2.5%  
567 Penicillin Streptomycin, 20µM L-Glutamine, and 100µM Beta 2-mercaptoethanol (Sigma-  
568 Aldrich). Cells were incubated for 18 hours without stimulus, or with the following stimuli:  
569 Lipopolysaccharide (LPS) (Invivogen) 100ng/ml(Sander *et al.*, 2017), IFNγ (Novaprotein)  
570 1000U/ml(Sander *et al.*, 2017), Polyinosinic:polycytidylic acid (poly(I:C)) (InvivoGen)  
571 25µg/ml(Farina *et al.*, 2004), Imiquimod (Insight Technology LTD) 20µg/ml, Peptidoglycan

572 (PGN) (InvivoGen) 10 $\mu$ g/ml), Pam2CGDPKHPKSF (FSL-1) (InvivoGen) (200ng/ml). After  
573 incubation, plates were spun to remove cellular debris, and supernatants were collected and  
574 stored at -80°C.

575 Cell culture supernatants were tested for the presence of 16 analytes using a custom  
576 10-plex Luminex ProcartaPlex assay (Thermo Fisher Scientific), and a custom 6-plex  
577 Luminex ProcartaPlex assay (Thermo Fisher Scientific) designed to profile the expression of:  
578 CCL2, CCL3, CCL4, CCL5, FGF-2, GM-CSF, IL-1 $\beta$ , IL-1RA, IL-6, IL-8, IL-10, MMP-9,  
579 Osteopontin, TIMP-1, TNF- $\alpha$  and VEGF-A. Samples were diluted in cell culture medium at a  
580 ratio of 1:1 for the 10-plex Luminex ProcartaPlex assay, and 1:40 for the 6-plex Luminex  
581 ProcartaPlex assay. The Luminex assays were performed according to manufacturer's  
582 instructions, and beads were ran on a Luminex LX-200 (Luminex), using xPONENT  
583 software (Luminex). Results were visualised using Prism 8 (GraphPad) and R version 3.5.1  
584 (The R Foundation).

585

### 586 **Phagocytosis assays**

587 Microsphere phagocytosis assay: Macrophages were placed in 1.5ml Eppendorfs, at  
588 10,000 cells in 100 $\mu$ l PBS and human serum opsonised Fluoresbrite™ Yellow Green  
589 Microspheres 1 $\mu$ m (Polysciences) were added at a concentration of 10:1 for 1 hour. Controls  
590 included cells cultured at 4°C and 37°C in the presence of 10 $\mu$ M cytochalasin D (Sigma-  
591 Aldrich).

592 E.coli phagocytosis assay: *E.coli* were grown until log-phase growth in and had  
593 reached an optical density (595nm) of 0.3. Bacteria were opsonised in heat-inactivated  
594 human serum for 30 minutes at 37°C and labelled via incubation with 10 $\mu$ M  
595 carboxyfluorescein succinimidyl ester (CFSE) (Biolegend) for 30 minutes at 37°C. Labelled  
596 bacteria were washed 3 times in PBS prior to use. First trimester placental cell suspensions



597 were plated at a density of  $1 \times 10^6$ /ml per well in PBS. Labelled *E.coli* were added at a MOI of  
598 10, and cultured for 1 hour at 37°C. Control wells were incubated at 4°C and at 37°C in  
599 presence of 10µM Cytochalasin-D. Plates were centrifuged at 200g for 5 minutes to promote  
600 cell-bacteria interactions. Cells were washed 3 times in 4°C PBS, and stained for flow  
601 cytometry as described above.

602

### 603 **Reactive oxygen species production assays**

604 FACS isolated HBC were plated at a density of 50,000 cells in 50µl of DMEM  
605 (Gibco) supplemented with 10% FBS (Sigma-Aldrich), 2.5% Penicillin Streptomycin, 20µM  
606 L-Glutamine. Cells were stained with 1µM CM-H2DCFDA (Thermo Fisher Scientific), and  
607 were either treated with 1x cell activation cocktail (PMA-ionomycin) (Biolegend) for 30  
608 minutes, or incubated without stimulation. Cells were washed in PBS and data acquired as  
609 described above.

610 *Ex-vivo* imaging of HBC ROS production was carried out by incubating placental villi  
611 with anti-CD64 antibody conjugated to PE and 1µM CM-H2DCFDA for 15 minutes. The  
612 villi were placed in Ibidi µ-Dish 35 mm and imaged using a Zeiss SP8 confocal LSM 700  
613 (Zeiss).

614

### 615 **Cathepsin B activity assay and acridine orange assay**

616 Macrophages were seeded at 10,000 cells/well in 10µl PBS on poly-L-lysine (Sigma)  
617 coated Ibidi 4 well µ-Dish plates. Zymosan bioparticles (Thermo Fisher Scientific) were  
618 added at a concentration of 10 particles per cell. Cathepsin B activity was determined using  
619 Magic Red™ (a cell-permeable and non-cytotoxic reagent that contains a cathepsin B target  
620 sequence peptide (RR)2 linked to a red (Cresyl Violet) fluorescent probe) and lysosomes  
621 were detected with acridine orange (Biorad), according to manufactures instructions.

622

### 623 **Phagosomal pH assay**

624 Placental macrophage phagosomal pH measurements were performed by adapting a  
625 method using the fluorescent-sensitive pH dye SNARF-1 (S-1) with a dual emission  
626 spectrum(Foote et al., 2017). Carboxy-S-1-succinimidyl ester (Thermo Fisher Scientific) was  
627 coupled to zymosan coated beads (Thermo Fisher Scientific) and opsonised with human  
628 serum. Macrophages were cultured at 10,000 cells/well in 10 $\mu$ l PBS, in poly-lysine (Sigma)  
629 coated Ibidi 4 well  $\mu$ -Dish plates. 5x10<sup>5</sup> S-1 labelled beads were added per well to  
630 macrophages. 50 $\mu$ g of Carboxy S-1-acetoxymethyl (S-1-AM) ester (Thermo Fisher  
631 Scientific) was added as a cytosolic dye (0.5  $\mu$ g/ml working solution). Subsequently, cells  
632 were examined under a 63x oil-immersion objective on a Zeiss SP8 confocal LSM 700  
633 (Zeiss), where cells were excited at 555 nm and emission was measured at 560-600 nm and  
634 600-610 nm. Over 100 measurements were made per condition. The pH scale was generated  
635 as described previously(Foote et al., 2017).

636

### 637 ***Escherichia coli* and *Lactobacillus crispatus* killing assays**

638 *E. coli* and *L. crispatus* were grown overnight in LB and Man, Rogosa and Sharpe  
639 (MRS) broth respectively. Bacteria were subcultured the following day until they had reached  
640 log-phase growth and an optical density (595nm) of 0.3. Bacteria were opsonised in heat-  
641 inactivated human serum for 30 minutes at 37°C. FACS purified placental cells were plated  
642 into 96 well plates at a density of 10,000 cells in 50 $\mu$ l of DMEM (Gibco) supplemented with  
643 10% FBS (Sigma-Aldrich), 20 $\mu$ M L-Glutamine and 25mM Hepes (Gibco). Bacteria were  
644 added at a MOI of 1 or 10, and plates were centrifuged at 200g for 5 minutes to promote cell-  
645 bacteria interactions. After incubation for 1 hour, cells were lysed in deionised water, and  
646 serial dilutions were plated onto LB agar or MRS agar plates, for *E. coli* and *L. crispatus*

647 experiments, respectively. Colony forming units (CFU) were counted after 24 hours for *E.*  
648 *coli* and after 48 hours for *L. crispatus*.

649

### 650 **Analysis of publicly available single-cell RNAseq data**

651 Single-cell RNA sequencing (scRNAseq) data of first trimester placenta(Vento-  
652 Tormo et al., 2018) was obtained at from EMBL-EBI ArrayExpress  
653 ([www.ebi.ac.uk/arrayexpress](http://www.ebi.ac.uk/arrayexpress)), under the experiment code E-MTAB-6701. Sequencing data  
654 from placental samples were aligned using the Cell Ranger Single-Cell Software Suite (v3.0,  
655 10x Genomics) against the GRCh38.93 human reference genome. Downstream analysis of  
656 each sample was performed using Seurat (v3.0)(Butler et al., 2018). Cells with fewer than  
657 500 detected genes, and more than 20% mitochondrial gene expression were removed.  
658 Samples were log-normalised and integrated following the Seurat v3 Integration workflow.  
659 Clusters were identified using the *FindNeighbours* and *FindClusters* functions in Seurat.  
660 Clusters were annotated on the basis of expression of known marker genes. Uniform  
661 Manifold Approximation and Projection (UMAP) dimensionality reduction was performed  
662 using the *RunUMAP* function in Seurat, with default parameters. Significantly differentially  
663 expressed gene (DEGs) were identified using the *FindMarkers* function, using the Wilcox  
664 rank sum test, corrected for multiple comparisons.

665 scRNAseq data from early human fetal immune cells was obtained from GEO under  
666 the accession code GSE133345. The dataset was analysed using Seurat, and subset to include  
667 only myeloid cells. These cells were integrated with HBC and PAMM clusters from the  
668 placenta scRNAseq dataset using the reference-based integration workflow in Seurat, using  
669 the early human fetal myeloid cell object as a reference. Pearson's correlations between  
670 annotated clusters were calculated using the average expression per cluster of the 2000  
671 variable genes used for integration. Cell cycle scoring of HBC was performed using the

672 *CellCycleScoring* function in Seurat, and predicted cell cycle states were overlaid onto  
673 UMAP embeddings.

674 Cell Ranger output files for each sample were analysed using Velocity(La Manno et  
675 al., 2018) (python version 0.17.17). Output loom files were merged with Seurat objects in R  
676 and RNA velocity vectors were calculated using the *RunVelocity* function from the  
677 SeuratWrappers package, and projected onto UMAP embeddings using the  
678 *show.velocity.on.embedding.cor* function from the VelocityR package.

679 Comparisons of cell type similarity between datasets was performed using a random  
680 forest model in the ranger R package, as previously described(Stewart et al., 2019). PBMC  
681 scRNAseq data for comparison was downloaded from 10x Genomics  
682 (<https://support.10xgenomics.com/single-cell-gene-expression/datasets>). Expression matrices  
683 from both datasets were subset using the union of the highly variable features detected in  
684 each dataset. The random forest model was built using the *ranger* function on the PBMC  
685 dataset and single-cell prediction scores were generated for placental cells using the *predict*  
686 function.

687 Single cell gene signature enrichment scores were calculated using the  
688 *AddModuleScore* function in Seurat. Gene signatures from the cirrhotic liver scar-associated  
689 macrophages (SAMacs) and Kupffer cells (KCs)(Ramachandran et al., 2019) were generated  
690 from the analysis of scRNAseq data obtained from GEO under the accession code  
691 GSE136103. In brief, the datasets were aligned and pre-processed as described above, and  
692 subset to include only the myeloid compartment. DEGs in SAMac and KC clusters were  
693 identified, and genes with log fold change > 0.5 and adjusted p value < 0.05 were used as  
694 gene signatures. DEGs were identified between yolk sac macrophages and embryonic  
695 monocytes (Bian et al., 2020), and the top fifty genes with log fold change > 0.5 and adjusted  
696 p value < 0.05 were used as the gene signatures for each population. The gene signature from

697 CS10 macrophages(Zeng et al., 2019) was generated from the analysis of scRNAseq data  
698 obtained from GEO under the accession code GSE135202. The data was processed as  
699 described above and subset to include endothelial and hematopoietic populations. DEGs in  
700 macrophages were identified, and the top fifty genes with log fold change > 0.5 and adjusted  
701 p value < 0.05 were used as the gene signature.

702 Pseudotime trajectory analysis of PAMM was performed with the Slingshot R  
703 package(Street et al., 2018), and the calculated trajectory was overlain onto the UMAP  
704 embeddings. Selected genes which varied across the slingshot trajectory were plotted as  
705 heatmaps of smoothed scaled gene expression. Smoothing was performed using the *rollmean*  
706 function in the zoo R package.

707

#### 708 **Cell-cell interactions analyses**

709 Predicted cell-cell ligand-receptor interactions were inferred from scRNAseq data  
710 using CellphoneDB (Efremova et al., 2020), using the online tool ([www.cellphonedb.org](http://www.cellphonedb.org)).  
711 The minimum proportion of cells in a cluster expressing a gene was set to 10%, and the  
712 number of iterations was set to 1000. Ligand-receptor pairs were subset to include only the  
713 16 ligands profiled in Luminex experiments. An estimate for interaction potential between  
714 cells was obtained by multiplying the log-normalised cytokine secretion of each ligand from  
715 sort-purified cell populations, by the average log-normalised gene expression of each  
716 receptor in each cluster.

717

#### 718 **Online Supplemental Material**

719 **Figure S1** shows the digestion protocols for obtaining single cell suspensions, HLA allotype  
720 staining for matched maternal blood and decidua, relating to Figure 1B, first trimester  
721 placental scRNAseq analysis, and the full gating strategy for the isolation of HBC and

722 PAMM populations. **Figure S2** shows the identification and characterisation of PAMM  
723 populations. **Figure S3** shows the data for cytokine, chemokine and growth factor secretion,  
724 related to Figure 5A, predicted interactions of HBC, PAMM1a and PAMM1b with other  
725 placental cells, quantification of TLR flow cytometric data related to Figure 5D, and TLR  
726 gene expression data. **Figure S4** shows the normalised cytokine, chemokine and growth  
727 factor secretion, related to Figure 5E. **Figure S5** shows the phagocytic and microbial capacity  
728 of HBC and PAMM1a. **Supplementary file 1** presents the gene signatures used for  
729 scRNAseq enrichment analyses, relating to Figures 2A, 2D and 4J. **Supplementary Table 1**  
730 provides a list of reagents, antibodies and software used throughout the study.

731

### 732 **Acknowledgements**

733 We thank the following for assistance: The Flow Cytometry Core Facility at the  
734 Department of Pathology and Core staff at the Immunophenotyping Hub at the Department of  
735 Medicine, University of Cambridge. Mike Hollinshead at the Microscopy Core at the  
736 Department of Pathology, Cambridge. Kjersti Aagaard from the Department of Obstetrics &  
737 Gynecology, Division of Maternal-Fetal Medicine, Baylor College of Medicine and Texas  
738 Children's Hospital, Houston Texas and Menna Clatworthy from the Department of  
739 Medicine, University of Cambridge for scientific discussion. Lucy Gardner, Imogen Duncan  
740 and Ritu Rani for their help in processing placental samples. We thank all donors who  
741 participated in this study and hospital staff.

742 This work was supported by the Wellcome Trust, Royal Society, Centre for  
743 Trophoblast Research, and Department of Pathology, University of Cambridge, UK. N.McG,  
744 is funded by a Wellcome Sir Henry Dale and Royal Society Fellowship (grant number  
745 204464/Z/16/Z). J.T is funded by a Wellcome Trust PhD Studentship (grant number  
746 215226/Z/19/Z). AS is funded by the MRC (grant number: MR/P001092/1).

747

748 **Author Contributions**

749           Conceptualisation: N.McG, J.T, A.S and A.M. Methodology: N.McG, J.T, X.Z, A.A,  
750 R.D, M.D, C.L, P.N, J.C and G.B. Formal analysis: N.McG, J.T, A.A, X.Z, R.D, M.D, C.L.  
751 and G.B. Intellectual input: N.McG, J.T, A.M, A.S, F.G, G.B, X.Z and R.S. Writing: N.McG,  
752 J.T, A.S and A.M. Visualisation: N.McG and J.T. Supervision: N.McG. All authors discussed  
753 the manuscript.

754

755 **Declaration of Interests**

756 The authors declare no competing interests.

757

758

759 **Figure Legends**

760 **Figure 1. Anti-HLA antibodies allow for the specific identification of Hofbauer cells by**  
761 **flow cytometry.**

762 (A) Schematic drawing of the human placenta and a villous cross-section. HBC – Hofbauer  
763 cells, EGA – Estimated gestational age. (B) Representative flow cytometric gating strategy  
764 identifying two placental macrophage populations based on HLA-DR expression. Blue gate –  
765 HLA-DR<sup>+</sup> macrophages. Red gate – HLA-DR<sup>-</sup> macrophages. (C) Differential expression of  
766 HLA-A3 within the CD14<sup>+</sup> macrophage gate, shown by biaxial plot and heatmap overlay.  
767 Maternal macrophages are indicated by the blue gate (HLA-DR<sup>+</sup>HLA-A3<sup>+</sup>), fetal  
768 macrophages are indicated by the red gate (HLA-DR<sup>-</sup>HLA-A3<sup>-</sup>). Bidirectional arrows depict  
769 equivalent cells. (D) Quantification of the abundance of PAMM within CD14<sup>+</sup> placental cell  
770 suspensions across the indicated EGA. Each data point indicates a separate donor (n=11). (E)  
771 Whole-mount immunofluorescence of a placental villus, where HBC stained with CD64 (red)  
772 are within villous stroma, and PAMM stained with HLA-DR (green, white arrow) are on the  
773 syncytial layer. Cell nuclei are stained with Hoechst (blue). Scale bar = 50µm. Representative  
774 image of n=3. (F) Scatterplot showing log-normalised gene expression of HBC (x-axis) and  
775 PAMM (y-axis) clusters derived from scRNAseq data analysis. Red dots represent genes that  
776 are differentially expressed with an adjusted p value <0.01 (Wilcox rank sum test). (G) Flow  
777 cytometric analysis of expression of indicated markers by HBC (identified with anti-HLA  
778 antibodies in red overlay) and PAMM (grey). Representative plots of n=3. Data are  
779 represented as mean ± SEM (D).

780

781 **Figure 2. First trimester HBC are transcriptionally similar to ‘primitive’ macrophages**  
782 **and proliferate *in situ*.**

783 (A) Heatmap of placental scRNAseq cluster mean enrichment scores for extra-embryonic



784 yolk sac (YS) macrophage and embryonic monocyte gene signatures(Bian et al., 2020). HBC  
785 – Hofbauer cell, PAMM – placenta-associated maternal monocytes/macrophages, VCT –  
786 villous cytotrophoblast, VCTp – proliferating villous cytotrophoblast, SCT –  
787 syncytiotrophoblast, EVT – Extravillous trophoblast, Fibro – Fibroblasts, Endo – Endothelial  
788 cells. (B) UMAP visualisation of 3,846 single cell transcriptomes from first trimester  
789 placenta and embryonic myeloid cells(Bian et al., 2020). pHBC – proliferating HBC, YSMP -  
790 yolk sac-derived myeloid-biased progenitors, GMP - granulocyte–monocyte progenitors,  
791 YS\_Mac – yolk sac macrophage. (C) Heatmap depicting transcriptomic similarity between  
792 annotated clusters. Clusters are ordered according to hierarchical clustering. HBC and  
793 YS\_Mac1 are highlighted in blue. (D) Violin plot of placental scRNAseq cluster enrichment  
794 scores for primitive macrophages from a Carnegie stage 10 (CS10) embryo(Zeng et al.,  
795 2019). (E) Violin plots of *HLA-DRB1* and *FOLR2* log-normalised gene expression in HBC,  
796 PAMM, YS\_Mac1 and CS10 macrophages. (F) Representative flow cytometric plot and  
797 quantification of Ki67 expression by HBC (n=8). (G) Representative immunohistochemistry  
798 analysis of Ki67 expression in placental tissue sections. Black arrowheads indicate Ki67<sup>+</sup>  
799 cells. Scale bar = 100µm. (H) Incorporation of 5-ethynyl-2'-deoxyuridine (EDU) into FACS-  
800 isolated HBC after 18 hour culture, with and without the addition of M-CSF (n= ≥4), *p*-value  
801 calculated by one-way ANOVA. (I) UMAP visualisation of 1,091 HBC single cell  
802 transcriptomes identifying two proliferating HBC populations. (J) Dotplot heatmap of log-  
803 normalised gene expression of genes associated with stages of the cell cycle in HBC clusters.  
804 Dot size represents fraction of cells with non-zero expression. (K) UMAP visualisation of  
805 HBC with cells coloured by predicted cell-cycle state, as determined by cell-cycle scoring,  
806 with RNA velocity vector field projection calculated from all genes in all cells (black arrows)  
807 overlain. Data are represented as mean ± SEM (F) or mean alone (H).  
808

809 **Figure 3. PAMM are a heterogeneous population, comprised of three subsets based on**  
810 **their expression of FOLR2, CD9 and CCR2 expression.**

811 (A) Expression of FOLR2 and HLA-DR by flow cytometry reveals three major populations  
812 of placental macrophages: HBC (red), PAMM1 (green) and PAMM2 (orange). (B) UMAP  
813 visualisation of 1,687 PAMM single cell transcriptomes from first trimester placenta, with  
814 overlays of *CD9* and *FOLR2* log-normalised gene expression. (C) Heterogeneous expression  
815 of CD9 within PAMM1 by flow cytometry. (D) Overlay flow cytometric plots of PAMM1  
816 (blue) and peripheral blood (PB) monocytes from matched maternal blood (red) of CD9 and  
817 CCR2 expression. (E) Flow cytometric plot of CD9 and CCR2 expression within PAMM1,  
818 showing representative gates for the identification of PAMM1a and PAMM1b. (F)  
819 Enumeration of HBC and PAMM populations as a percentage of total CD14<sup>+</sup> cells from  
820 placental cell suspensions (n=11). *p*-values were calculated by one-way ANOVA with  
821 Tukey's multiple-comparisons test. (G) Representative Giemsa-Wright stained cytopins of  
822 HBC and PAMM subsets isolated by FACS. Scale bars = 20µm. (H) Forward scatter (FSC-  
823 A) and (I) Side scatter (SSC-A) mean fluorescence intensity (MFI) of HBC and PAMM  
824 subsets. *p*-values were calculated by one-way ANOVA with Tukey's multiple-comparisons  
825 test. Data are represented as mean ± SEM (F) or mean alone (H, I). \**p* ≤ 0.05, \*\*\*\**p* ≤  
826 0.0001.

827

828 **Figure 4. PAMM1 undergo a monocyte-to-macrophage transition and adopt a tissue-**  
829 **repair phenotype on the placental surface.**

830 (A) UMAP visualisation of 1,687 PAMM single cell transcriptomes with Slingshot trajectory  
831 overlain. (B) Heatmaps of smoothed scaled gene expression of selected genes which are  
832 downregulated and (C) upregulated during PAMM1b to PAMM1a differentiation, ordered  
833 according to Slingshot trajectory. (D) Relative surface expression of markers identified in (C)

834 in PAMM1a (green) and PAMM1b (cyan), compared to FMO control (grey), measured by  
835 flow cytometry. Representative plots of n=3. (E) Transmission electron microscopy of first  
836 trimester placental villous cross-section, PAMM1a can be observed on the placental surface,  
837 localised to sites of damage to the syncytial layer (red inset). PAMM1a are loaded with lipid  
838 droplets (yellow arrows). Scale bars = 20µm. (F) Identification of CD9<sup>+</sup> (green) HLA-DR<sup>+</sup>  
839 (red) PAMM1a cells on the surface of a 9wk EGA placental sample by fluorescence  
840 microscopy. Representative image of n=3. Cell nuclei are stained with DAPI (blue). Scale  
841 bars = 20µm. (G) Secretion of MMP-9 by FACS-isolated PAMM1a and PAMM1b after  
842 overnight culture (n=6). *p*-value calculated by unpaired t-test. (H) Log-normalised gene  
843 expression of fibronectin (*FNI*) in PAMM1a and PAMM1b clusters, as determined from  
844 scRNAseq data. (I) Analysis of intracellular neutral lipid content by flow cytometry  
845 following staining with BODIPY; mean fluorescence intensity (MFI) of HBC and PAMM  
846 subsets is shown. *p*-values calculated by one-way ANOVA with Tukey's multiple-  
847 comparisons test. (J) Heatmap of placental macrophage mean enrichment scores for Kupffer  
848 cells (KC) and scar-associated macrophage (SAMac) gene signatures (Ramachandran et al.,  
849 2019). Data are represented as mean ± SEM. \*\**p* ≤ 0.01, \*\*\**p* ≤ 0.001.

850

851 **Figure 5. HBC and PAMM subsets display distinct cytokine secretion profiles at the**  
852 **steady state and in response to TLR stimulation.**

853 (A) Heatmap of average scaled cytokine, chemokine and growth factor secretion from FACS-  
854 isolated HBC, PAMM1a and PAMM1b after overnight culture without stimulation (n=6). (B)  
855 Schematic representation of inferred cell-cell interactions from Luminex and scRNAseq data.  
856 Lower panel shows an example of predicted interactions between HBC and other placental  
857 cells based on VEGF-A and KDR. (C) Heatmap of predicted interactions between HBC (red)  
858 and other placental cell populations (blue). Interaction potentials were calculated from

859 expression of ligands determined by protein secretion, and scRNAseq expression of cognate  
860 receptors. (D) Relative flow cytometric expression of TLRs in HBC, PAMM1a and  
861 PAMM1b compared to FMO control (grey). Plots are representative of n=3. (E) Heatmaps  
862 showing the fold-change in cytokine secretion of FACS-isolated HBC, PAMM1a and  
863 PAMM1b cultured overnight with TLR stimulation, relative to no stimulation (n=6). *p*-values  
864 were calculated by two-way ANOVA with Dunnett's multiple-comparisons test. \**p* ≤ 0.05,  
865 \*\**p* ≤ 0.01, \*\*\**p* ≤ 0.001, \*\*\*\**p* ≤ 0.0001.

866

867 **Figure 6. HBC are capable of mounting a microbicidal response.**

868 (A) Phagocytosis of YG beads by FACS-isolated HBC and PAMM1a measured by flow  
869 cytometry. *p*-values were calculated by two-way ANOVA with Tukey's multiple-  
870 comparisons test. (B) Whole-mount immunofluorescence microscopy of a placental villus  
871 showing CD64 expression (red) and ROS-dependant probe CM-H2DCFDA (green). Edges of  
872 villus are indicated by white lines. Right panels, magnification of individual cells, denoted by  
873 symbols. Scale bars = 20µm. (C) Relative expression of cathepsin B in HBC and PAMM1a  
874 to FMO control (grey), measured by flow cytometry. (D) Cathepsin B activity in FACS-  
875 isolated HBC, co-cultured with zymosan particles, determined by cathepsin B Magic Red™  
876 staining. Scale bars = 20µm. (E) Acridine orange staining of lysosomes in FACS-isolated  
877 HBC, co-cultured with zymosan particles. Scale bars = 20µm. (F, G) Comparison of the  
878 phagosomal pH of HBC and PAMM1a. (F) Representative images of phagosomal pH of  
879 FACS-isolated HBC and PAMM1a after coculture with Carboxy SNARF®-1 -labelled  
880 zymosan particles for 20 minutes. The cytosol is labelled with 5-(and-6)-carboxy S-1  
881 acetoxymethyl (S-1-AM) ester, a cell-permeant pH indicator. Right panel, pH scale. (G)  
882 Quantification of phagosomal pH, each data point represents an average of >100  
883 measurements per separate donor. n≥3. *p*-value was calculated by unpaired t-test. (H, I) Rates

884 of *Lactobacillus crispatus* (H) and *Escherichia coli* (I) killing by HBC and PAMM1a after 1  
885 hour co-culture at a MOI of 1, relative to negative control, where no macrophages were  
886 added.  $p$ -values were calculated by one sample t-test. Each data point indicates a separate  
887 donor. (J) Schematic depicting locations and subset-specific roles of placental macrophages.  
888 Data are represented as mean  $\pm$  SEM. <sup>ns</sup> $p > 0.05$ , \*\* $p \leq 0.01$ , \*\*\* $p \leq 0.001$ , \*\*\*\* $p \leq 0.0001$ .  
889

890 **Supplementary Data**

891 **Figure S1. Isolation and characterisation of placental macrophage populations.**

892 (A) Schematic representation of a digestion protocol used to isolate placental cells (Tang et  
893 al., 2011). (B, C) Flow cytometric analysis of fetal myeloid cells (HLA-A2<sup>+</sup>), from the same  
894 sample digested with either trypsin alone (B), or (C) trypsin and collagenase. HBC (black  
895 gate) and PAMM are identified in both steps of the digestion process. (D, E) Flow cytometric  
896 analysis of maternal peripheral blood monocytes (D) and decidual CD14<sup>+</sup> cells (E), matched  
897 with the placental sample shown in Figure 1 B, C. (F) UMAP visualisation of 22,618  
898 placental single cell transcriptomes (Vento-Tormo et al., 2018). VCT – villous  
899 cytotrophoblast, VCTp – proliferating villous cytotrophoblast, SCT – syncytiotrophoblast,  
900 EVT – Extravillous trophoblast, Fibro – Fibroblasts, Endo – Endothelial cells. (G) UMAP  
901 visualisation with overlays of *CD68* and *HLA-DRB1* log-normalised gene expression. (H)  
902 Violin plots showing log-normalised gene expression of *RSP4Y1* and *XIST*, for one male fetal  
903 donor from scRNAseq dataset. (I) Flow cytometric plots showing the gating strategy and  
904 representative Ki67 staining for HBC (n=8). (J) Representative flow cytometric plots for  
905 gating strategy used to isolate HBC and PAMM populations for phenotypic, morphological  
906 and functional analysis. For the donor shown, maternal and fetal cells are HLA-A3<sup>+</sup> and  
907 HLA-A3<sup>-</sup> respectively.

908

909 **Figure S2. Identification of PAMM populations.**

910 (A) Flow cytometric analysis of decidual CD14<sup>+</sup> cells. Cells with a phenotype consistent with  
911 PAMM2 (FOLR2<sup>+</sup> HLA-DR<sup>+</sup>) (red gate) and PAMM1b (blue gate) were readily identified.  
912 Cells with a phenotype consistent with PAMM1a were low in abundance (green gate).  
913 Representative flow cytometric plots from n=3 experiments. (B) Identification of HLA-DR<sup>+</sup>  
914 (red) FOLR2<sup>+</sup> (green) macrophages in the decidua by fluorescence microscopy. Cell nuclei

915 are stained with DAPI (blue). Scale bar = 50 $\mu$ m. Representative image of n=2. (C) UMAP  
916 visualisation of 9,474 myeloid cells from placenta, decidua and maternal blood(Vento-Tormo  
917 et al., 2018). Cells are coloured and labelled by cluster identity (left panel) and tissue of  
918 origin (right panel). cDC1 – conventional type 1 dendritic cells, cDC2 – conventional type 2  
919 dendritic cells, C mono – classical monocytes, dMac1 – decidual macrophages 1, dMac2 –  
920 decidual macrophages 2, dMono – decidual monocytes, pDC – plasmacytoid dendritic cells,  
921 pHBC/pdMac2 - proliferating HBC and dMac2, NC Mono – non-classical monocytes. (D)  
922 Violin plots showing log-normalised gene expression of *FOLR2* and *HLA-DRB1* in placental,  
923 decidual and maternal blood myeloid cells. (E) Annotation of PAMM2 (placental cells within  
924 dMac2 cluster) (blue) onto original UMAP embedding of HBC and PAMM from the  
925 placental scRNAseq dataset (Figure S1F). (F) Heatmap of transcriptional similarity between  
926 placental macrophage/monocytes cell clusters and indicated PBMC populations, as  
927 determined using a random forest classification prediction. p-HBC – proliferating HBC. (G)  
928 Scatterplot showing log-normalised gene expression of PAMM1b (x-axis) and maternal  
929 blood classical monocytes (y-axis) clusters. Red dots represent genes that are differentially  
930 expressed with an adjusted p value <0.01 (Wilcox rank sum test). (H) Scanning electron  
931 micrographs of PAMM1a on the surface of a first trimester placenta, adhering to a site of  
932 damage on a branching villus. Scale bars = 20 $\mu$ m. (I) Representative flow cytometric  
933 histograms of BODIPY staining within HBC and PAMM subsets, compared to unstained  
934 cells (grey). (J) Images of BODIPY staining of FACS-isolated PAMM1a and PAMM1b.  
935 Scale bars = 20 $\mu$ m. Representative images of n=2.

936

937 **Figure S3. HBC, PAMM1a and PAMM1b secretome analysis in the steady-state and**  
938 **TLR expression.**

939 (A) Cytokine, chemokine and growth factor secretion of FACS-isolated HBC, PAMM1a and  
940 PAMM1b after 18 hours in culture without stimulation, profiled by Luminex (n=6). *p*-values  
941 calculated by one-way ANOVA with Tukey's multiple-comparisons test. Only significant *p*-  
942 values, and *p*-values approaching significance shown. (B) Heatmap of predicted interactions  
943 between HBC, PAMM1a and PAMM1b (red) and other placental cell populations (blue).  
944 Interaction potentials were calculated from expression of ligands determined by protein  
945 secretion, and scRNAseq expression of cognate receptors. (C) Whole-mount  
946 immunofluorescence of placental villi stained for CD206 (red), and CD31 (green). Images  
947 from 2 independent donors, both 9wk EGA. Scale bar = 100µm. (D) Quantification of  
948 expression of TLRs in HBC, PAMM1a and PAMM1b, profiled by flow cytometry, n=3. (E)  
949 Dotplot heatmap of log-normalised gene expression of TLR genes in HBC and PAMM  
950 scRNAseq clusters. Dot size represents fraction of cells with non-zero expression. TLR9 was  
951 not detected in the analysis. Data are represented as mean ± SEM.

952

953 **Figure S4. HBC, PAMM1a and PAMM1b secretome analysis in response to TLR**  
954 **stimulation.**

955 Normalised cytokine, chemokine and growth factor secretion of FACS-isolated HBC,  
956 PAMM1a and PAMM1b after 18 hours in culture with TLR stimulation, relative to without  
957 stimulation. HBC (red), PAMM1a (green), PAMM1b (cyan). Profiled by Luminex (n=6).  
958 Data are represented as mean ± SEM.

959

960 **Figure S5. Phagocytic and anti-bacterial capacity of HBC and PAMM1a.**

961 (A) Flow cytometric plots of scavenger receptor expression in HBC (red) and PAMM (grey).  
962 Representative flow cytometric plots of n=3 experiments. (B) Phagocytosis of CFSE-labelled  
963 *Escherichia coli* (*E. coli*) by HBC, PAMM1a, PAMM1b and PAMM2 subsets measured by



964 flow cytometry.  $p$ -values were calculated by two-way ANOVA with Tukey's multiple-  
965 comparisons test. (C) Representative flow cytometric plot of CM-H2DCFDA staining in  
966 FACS-isolated HBC with no stimulation (black) and with phorbol 12-myristate 13-acetate  
967 (PMA) (red), relative to no stain (grey) Representative plot from  $n=3$  experiments. (D)  
968 Cathepsin B activity, determined by cathepsin B Magic Red<sup>TM</sup> staining, and acridine orange  
969 staining of lysosomes in FACS-isolated PAMM1a, co-cultured with zymosan particles. Scale  
970 bars =  $20\mu\text{m}$ . (E, F) Rates of *Lactobacillus crispatus* (*L. crispatus*) (E) and *E. coli* (F) killing  
971 by HBC and PAMM1a after 1 hour co-culture at a MOI of 10, relative to negative control,  
972 where no cells were added.  $p$ -values were calculated by one sample t-test.  $n \geq 2$ . Data are  
973 represented as mean  $\pm$  SEM. <sup>ns</sup> $p > 0.05$ , \* $p \leq 0.05$ , \*\*\*\* $p \leq 0.0001$ .  
974

975 **Supplementary Table 1. Antibodies, reagents and software used.**

REAGENT or RESOURCE	SOURCE	IDENTIFIER
Antibodies		
Anti-Human Arginase 2 (clone poly)	Abcam	Cat#:ab81505, RRID:AB_1861680
Anti-Human AXL (APC) (clone 108724)	R&D Systems	Cat#:FAB154A, no RRID
Anti-Human Cathepsin D (unconjugated) (clone poly)	Thermo Fischer Scientific	Cat#:PA5-17353, RRID:AB_1098141 8
Anti-Human CCR2 (BV421) (clone K036C2)	BioLegend	Cat#:357209, RRID:AB_2562293
Anti-Human CCR2 (PE) (clone K036C2)	BioLegend	Cat#:357205, RRID:AB_2562058
Anti-Human CD14 (PE/Dazzle) (clone HCD14 )	BioLegend	Cat#:325634, RRID:AB_2563625
Anti-Human CD163 (PE/Cy7) (clone GHI/61)	BioLegend	Cat#:333613, RRID:AB_2562640
Anti-Human CD19 (FITC) (clone SJ25C1)	BioLegend	Cat#:363008, RRID:AB_2564171
Anti-Human CD20 (FITC) (clone 2H7)	BioLegend	Cat#:302304, RRID:AB_314252
Anti-Human CD206 (PE) (clone 15-2)	BioLegend	Cat#:321105, RRID:AB_571910
Anti-Human CD206 (PerCP/Cy5.5) (clone 15-2)	BioLegend	Cat#:321121, RRID:AB_1090099 0

Anti-Human CD282 (TLR2) (PE) (clone TL2.1)	BioLegend	Cat#:309707, RRID:AB_314777
Anti-Human CD283 (TLR3) (PE) (clone TLR-104)	BioLegend	Cat#:315005, RRID:AB_2303469
Anti-Human CD284 (TLR4) (PE) (clone HTA125)	BioLegend	Cat#:312805, RRID:AB_314954
Anti-Human CD286 (TLR6) (PE) (clone TLR 6.127)	BioLegend	Cat#:334707, RRID:AB_2205398
Anti-Human CD289 (TLR9) (PE) (clone S16013D)	BioLegend	Cat#:394803, RRID: AB_280103
Anti-Human CD3 (FITC) (clone UCHT1)	BioLegend	Cat#:300406, RRID:AB_314060
Anti-Human CD31 (AF488) (clone WM59)	BioLegend	Cat#:303109, RRID:AB_493075
Anti-Human CD335 (FITC) (clone 9E2)	BioLegend	Cat#:331921, RRID:AB_2561964
Anti-Human CD36 (FITC) (clone 5-271)	BioLegend	Cat#:336203, RRID:AB_1575029
Anti-Human CD365 (TIM-1) (APC) (clone 1D12)	BioLegend	Cat#:353905, RRID:AB_2564324
Anti-Human CD45 (BUV395) (clone HI30)	BioLegend	Cat#:563792, RRID:AB_2744400
Anti-Human CD45 (BV605) (clone HI30)	BioLegend	Cat#:304042, RRID:AB_2562106
Anti-Human CD45 (PerCP/Cy5.5) (clone 2D1)	BioLegend	Cat#:368503, RRID:AB_2566351

Anti-Human CD56 (FITC) (clone HCD56)	BioLegend	Cat#:318304, RRID:AB_604100
Anti-Human CD63 (AF647) (clone H5C6)	BioLegend	Cat#:353015, RRID:AB_2561662
Anti-Human CD64 (BV605) (clone 10.1)	BioLegend	Cat#:305033, RRID:AB_2566236
Anti-Human CD64 (PE) (clone 10.1)	BioLegend	Cat#:305007, RRID:AB_314491
Anti-Human CD66b (AF700) (clone G10F5)	BioLegend	Cat#:305113, RRID:AB_2566037
Anti-Human CD66b (FITC) (clone G10F5)	BioLegend	Cat#:305103, RRID:AB_314495
Anti-Human CD68 (PE) (clone Y1/82A)	BioLegend	Cat#:333807, RRID:AB_1089057
Anti-Human CD9 (FITC) (clone HI9a)	BioLegend	Cat#:312103, RRID:AB_314908
Anti-Human CD9 (PE/cy7) (clone HI9a)	BioLegend	Cat#:312115, RRID:AB_2728255
Anti-Human FOLR2 (APC) (clone 94b/FOLR2)	BioLegend	Cat#:391705, RRID:AB_2721302
Anti-Human FOLR2 (PE) (clone 94b/FOLR2)	BioLegend	Cat#:391703, RRID:AB_2721335
Anti-Human HLA-A2 (APC/Cy7) (clone BB7.2)	BioLegend	Cat#:343310, RRID:AB_2561568
Anti-Human HLA-A3 (APC) (clone GAP.A3)	Thermo Fischer Scientific	Cat#:17-5754-42, RRID:AB_2573220

Anti-Human HLA-A3 (BV650) (clone GAP.A3)	BD Biosciences	Cat#:747774, RRID:AB_2739760
Anti-Human HLA-B7 (Biotin) (clone REA176)	Miltenyi Biotec	Cat#:130-106-046, RRID:AB_2652117
Anti-Human HLA-B7 (PE) (clone BB7.1)	BioLegend	Cat#:372403, RRID:AB_2650773
Anti-Human HLA-DR (APC) (clone L243)	BioLegend	Cat#:307605, RRID:AB_314683
Anti-Human HLA-DR (BV711) (clone L243)	BioLegend	Cat#:307643, RRID:AB_1121879 4
Anti-Human HLA-DR (BV786) (clone G46 - 6)	BD Biosciences	Cat#:564041, RRID:AB_2738559
Anti-Human HLA-DR (FITC) (clone G46 - 6)	BioLegend	Cat#:327006, RRID:AB_893569
Anti-Human HLA-DR (PE) (clone L243)	BioLegend	Cat#:307609, RRID:AB_314687
Anti-Human Ki67 (PE) (clone SolA15)	Thermo Fischer Scientific	Cat#:12569882, RRID:AB_1115095 4
Anti-Human Ki67 (Unconjugated) (clone Ki-67)	BioLegend	Cat#:350501, RRID:AB_1066274 9
Anti-Human LOX1 (BV421) (clone 15C4)	BioLegend	Cat#:358609, RRID:AB_2728342
Anti-Human Lysozyme (FITC) (clone LZ-2)	Thermo Fischer Scientific	Cat#:GIC207, RRID:AB_2536533

Anti-Human TLR7 (PE) (clone 4G6)	Thermo Fischer Scientific	Cat#:MA5-16249, RRID:AB_2537767
Anti-Human TLR8 (PE) (clone 44C143)	Abcam	Cat#:ab45097, RRID:AB_778508
<b>Bacterial and Virus Strains</b>		
<i>Lactobacillus crispatus</i>	ATCC	ATCC-33820
<b>Chemicals, Peptides, and Recombinant Proteins</b>		
3,3'-diaminobenzidine (DAB)	Sigma-Aldrich	D4168-50SET
4',6-diamidino-2-phenylindole (DAPI)	Sigma-Aldrich	D9542
Acetone	Sigma-Aldrich	179124-1L
Aqua Zombie Fixable Viability Kit	Biologend	423101
BD Difco™ Dehydrated Culture Media: Lactobacilli MRS Agar	Thermo Fischer Scientific	DF0882-17-0
BD Difco™ Lactobacilli MRS Broth	Thermo Fischer Scientific	11713553
BD Pharmingen Transcription Factor Buffer	BD bioscience	562574
Beta 2-mercaptoethanol	Sigma-Aldrich	444203
BODIPY 493/503	Thermo Fisher Scientific	D3922
BSA	Sigma-Aldrich	A9418
Carazzi's hematoxylin	Clin-Tech Ltd	642305
5-(and-6)-Carboxy SNARF-1, Acetoxymethyl Ester, Acetate	Thermo Fischer Scientific	C1272
SNARF™-1 Carboxylic Acid, Acetate, Succinimidyl Ester	Thermo Fischer Scientific	S22801
Carboxyfluorescein succinimidyl ester (CFSE)	Biologend	423801

Cell activation cocktail	Biolegend	423301
CM-H2DCFDA	Thermo Fischer Scientific	C6827
Collagenase V	Sigma-Aldrich	C9263
Cytochalasin-D	Sigma-Aldrich	C8273
DNase I	Roche	10104159001
Advanced DMEM/F-12	Thermo Fisher Scientific	12634028
EDTA	Sigma-Aldrich	324506
Fetal Bovine Serum	Sigma-Aldrich	f9665-500ML
Fluoresbrite™ Yellow Green Microspheres 1 μm	Polysciences	17154
Gibco™ HEPES (1M)	Thermo Fischer Scientific	11560496
Giemsa-stain	Sigma-Aldrich	48900-500ML-F
Glycerol gelatin	Sigma-Aldrich	GG1-15ML
Hoechst 33342 dye	Abcam	ab228551
Human AB serum	Sigma-Aldrich	H4522
Ibidi 4 well m-Dish plates	ibidi	80406
IFN-gamma	ThermoFisher	PHC4031
Imiquimod	InvivoGen	Tlrl-imqs
Invitrogen Zyomosan A Bioparticles	Thermo Fisher Scientific	Z2849
L-Glutamine	Sigma-Aldrich	G7513
<i>Lactobacillus crispatus</i>	ATCC	ATCC-33820
Lipopolysaccharide	Invivogen	tlrl-b5lps

Methanol	Thermo Fischer Scientific	10675112
Mouse serum	Sigma-Aldrich	M5905
optimal cutting temperature embedding medium	Thermo Fisher Scientific	12678646
Pam2CGDPKHPKSF (FSL-1)	Invivogen	ttrl-fsl
Pancoll	Pan-Biotech	P04-60500
Paraformaldehyde	Thermo Fisher Scientific	43368
Penicillin Streptomycin	Sigma-Aldrich	P4333
Peptidoglycan	Invivogen	ttrl-pgns2
Poly-L-lysine	Sigma-Aldrich	P4707
Polyinosinic:polycytidylic acid (poly(I:C))	Invivogen	ttrl-pau
Rat serum	Sigma-Aldrich	R9759-5ML
Triton X-100	Sigma-Aldrich	X100-500ML
Trypsin	Pan-Biotech	P10-025100P
VECTASHIELD® Antifade Mounting Medium with DAPI	Vector Laboratories	H-1200
VECTASTAIN® Elite® ABC HRP Kit	Vector Laboratories	PK-6100
Wright-stain	Sigma-Aldrich	WS16-500ML
Critical Commercial Assays		
Click-IT™ Plus EdU Alexa Fluor™ 647 Flow Cytometry Assay Kit	Thermo Fisher Scientific	C10634
10-plex Luminex ProcartaPlex assay	Thermo Fisher Scientific	PPX-10



6-plex Luminex ProcartaPlex assay	Thermo Fisher Scientific	PPX-06
Magic Red™ Cathepsin assay kit	BIO-RAD	ICT937
Software and Algorithms		
Flowjo v10.6.1	Treestar	<a href="https://www.flowjo.com/">https://www.flowjo.com/</a>
R version 3.5.1	The R foundation	<a href="https://www.r-project.org/">https://www.r-project.org/</a>
Seurat v3	Butler et al., 2018	<a href="https://satijalab.org/seurat/">https://satijalab.org/seurat/</a>
Velocyto & VelocytoR	La Manno et al., 2018	<a href="https://github.com/velocyto-team/velocyto.R">https://github.com/velocyto-team/velocyto.R</a>
gProfiler web tool	Reimand et al., 2016	<a href="https://biit.cs.ut.ee/gprofiler/gost">https://biit.cs.ut.ee/gprofiler/gost</a>
Slingshot R package v1.1.3	Street et al., 2018	<a href="https://github.com/ksreet13/slinsshot">https://github.com/ksreet13/slinsshot</a>
CellphoneDB	Efremova et al., 2020	<a href="https://www.cellphonedb.org/">https://www.cellphonedb.org/</a>

976

977

- 978 Bibliography  
979
- 980 Arany, E., and D.J. Hill. 1998. Fibroblast growth factor-2 and fibroblast growth factor  
981 receptor-1 mRNA expression and peptide localization in placentae from normal and  
982 diabetic pregnancies. *Placenta*. doi:10.1016/S0143-4004(98)90001-7.
- 983 Bian, Z., Y. Gong, T. Huang, C.Z.W. Lee, L. Bian, Z. Bai, H. Shi, Y. Zeng, C. Liu, J. He, J.  
984 Zhou, X. Li, Z. Li, Y. Ni, C. Ma, L. Cui, R. Zhang, J.K.Y. Chan, L.G. Ng, Y. Lan, F.  
985 Ginhoux, and B. Liu. 2020. Deciphering human macrophage development at single-cell  
986 resolution. *Nature*. doi:10.1038/s41586-020-2316-7.
- 987 Böckle, B.C., E. Sölder, S. Kind, N. Romani, and N.T. Sepp. 2008. DC-SIGN+ CD163+  
988 Macrophages Expressing Hyaluronan Receptor LYVE-1 Are Located within Chorion  
989 Villi of the Placenta. *Placenta*. doi:10.1016/j.placenta.2007.11.003.
- 990 Boyd, J.D., W.J. Hamilton, J.D. Boyd, and W.J. Hamilton. 1970. Stroma of Villi. *In The*  
991 *Human Placenta*.
- 992 Bulmer, J.N., L. Morrison, and J.C. Smith. 1988. Expression of class II MHC gene products  
993 by macrophages in human uteroplacental tissue. *Immunology*.
- 994 Burton, G.J. 1986. Scanning electron microscopy of intervillous connections in the mature  
995 human placenta. *J. Anat.*
- 996 Burton, G.J., D.S. Charnock-Jones, and E. Jauniaux. 2009a. Regulation of vascular growth  
997 and function in the human placenta. *Reproduction*. doi:10.1530/REP-09-0092.
- 998 Burton, G.J., and A.L. Watson. 1997. The structure of the human placenta: Implications for  
999 initiating and defending against virus infections. *Rev. Med. Virol.*  
1000 doi:10.1002/(SICI)1099-1654(199712)7:4<219::AID-RMV205>3.0.CO;2-E.
- 1001 Burton, G.J., A.W. Woods, E. Jauniaux, and J.C.P. Kingdom. 2009b. Rheological and  
1002 Physiological Consequences of Conversion of the Maternal Spiral Arteries for  
1003 Uteroplacental Blood Flow during Human Pregnancy. *Placenta*.  
1004 doi:10.1016/j.placenta.2009.02.009.
- 1005 Butler, A., P. Hoffman, P. Smibert, E. Papalexli, and R. Satija. 2018. Integrating single-cell  
1006 transcriptomic data across different conditions, technologies, and species. *Nat.*  
1007 *Biotechnol.* doi:10.1038/nbt.4096.
- 1008 Castellucci, M., A. Celona, H. Bartels, B. Steininger, V. Benedetto, and P. Kaufmann. 1987.  
1009 Mitosis of the Hofbauer cell: Possible implications for a fetal macrophage. *Placenta*.  
1010 doi:10.1016/0143-4004(87)90040-3.
- 1011 Costa, M.L., M.L. Robinette, M. Bugatti, M.S. Longtine, B.N. Colvin, E. Lantelme, W.  
1012 Vermi, M. Colonna, D.M. Nelson, and M. Cella. 2017. Two distinct myeloid subsets at  
1013 the term human fetal-maternal interface. *Front. Immunol.*  
1014 doi:10.3389/fimmu.2017.01357.

- 1015 D'Avila, H., C.G. Freire-de-Lima, N.R. Roque, L. Teixeira, C. Barja-Fidalgo, A.R. Silva,  
1016 R.C.N. Melo, G.A. DosReis, H.C. Castro-Faria-Neto, and P.T. Bozza. 2011. Host cell  
1017 lipid bodies triggered by *Trypanosoma cruzi* infection and enhanced by the uptake of  
1018 apoptotic cells are associated with prostaglandin E2 generation and increased parasite  
1019 growth. *J. Infect. Dis.* doi:10.1093/infdis/jir432.
- 1020 Dai, J., L. Peng, K. Fan, H. Wang, R. Wei, G. Ji, J. Cai, B. Lu, B. Li, D. Zhang, Y. Kang, M.  
1021 Tan, W. Qian, and Y. Guo. 2009. Osteopontin induces angiogenesis through activation  
1022 of PI3K/AKT and ERK1/2 in endothelial cells. *Oncogene.* doi:10.1038/onc.2009.189.
- 1023 Efremova, M., M. Vento-Tormo, S.A. Teichmann, and R. Vento-Tormo. 2020.  
1024 CellPhoneDB: inferring cell–cell communication from combined expression of multi-  
1025 subunit ligand–receptor complexes. *Nat. Protoc.* doi:10.1038/s41596-020-0292-x.
- 1026 Fagerberg, L., B.M. Hallstrom, P. Oksvold, C. Kampf, D. Djureinovic, J. Odeberg, M.  
1027 Habuka, S. Tahmasebpoor, A. Danielsson, K. Edlund, A. Asplund, E. Sjostedt, E.  
1028 Lundberg, C.A.K. Szigartyo, M. Skogs, J. Ottosson Takanen, H. Berling, H. Tegel, J.  
1029 Mulder, P. Nilsson, J.M. Schwenk, C. Lindskog, F. Danielsson, A. Mardinoglu, A.  
1030 Sivertsson, K. Von Feilitzen, M. Forsberg, M. Zwahlen, I. Olsson, S. Navani, M. Huss,  
1031 J. Nielsen, F. Ponten, and M. Uhlen. 2014. Analysis of the human tissue-specific  
1032 expression by genome-wide integration of transcriptomics and antibody-based  
1033 proteomics. *Mol. Cell. Proteomics.* doi:10.1074/mcp.M113.035600.
- 1034 Flannagan, R.S., B. Heit, and D.E. Heinrichs. 2015. Antimicrobial mechanisms of  
1035 macrophages and the immune evasion strategies of *Staphylococcus aureus*. *Pathogens.*  
1036 doi:10.3390/pathogens4040826.
- 1037 Foote, J.R., A.P. Levine, P. Behe, M.R. Duchon, and A.W. Segal. 2017. Imaging the  
1038 neutrophil phagosome and cytoplasm using a ratiometric pH indicator. *J. Vis. Exp.*  
1039 doi:10.3791/55107.
- 1040 Foote, J.R., A.A. Patel, S. Yona, and A.W. Segal. 2019. Variations in the phagosomal  
1041 environment of human neutrophils and mononuclear phagocyte subsets. *Front.*  
1042 *Immunol.* doi:10.3389/fimmu.2019.00188.
- 1043 Ford, H.Z., H.M. Byrne, and M.R. Myerscough. 2019. A lipid-structured model for  
1044 macrophage populations in atherosclerotic plaques. *J. Theor. Biol.*  
1045 doi:10.1016/j.jtbi.2019.07.003.
- 1046 Ginhoux, F., M. Greter, M. Leboeuf, S. Nandi, P. See, S. Gokhan, M.F. Mehler, S.J. Conway,  
1047 L.G. Ng, E.R. Stanley, I.M. Samokhvalov, and M. Merad. 2010. Fate mapping analysis  
1048 reveals that adult microglia derive from primitive macrophages. *Science (80-. ).*  
1049 doi:10.1126/science.1194637.
- 1050 Ginhoux, F., and M. Guilliams. 2016. Tissue-Resident Macrophage Ontogeny and  
1051 Homeostasis. *Immunity.* 44:439–449. doi:10.1016/j.immuni.2016.02.024.
- 1052 Goldstein, J., M. Braverman, C. Salafia, and P. Buckley. 1988. The phenotype of human

- 1053 placental macrophages and its variation with gestational age. *Am. J. Pathol.* 133:648–  
1054 659.
- 1055 Gomez Perdiguero, E., K. Klapproth, C. Schulz, K. Busch, E. Azzoni, L. Crozet, H. Garner,  
1056 C. Trouillet, M.F. De Bruijn, F. Geissmann, and H.R. Rodewald. 2015. Tissue-resident  
1057 macrophages originate from yolk-sac-derived erythro-myeloid progenitors. *Nature*.  
1058 doi:10.1038/nature13989.
- 1059 Hammond, M.E., G.R. Lapointe, P.H. Feucht, S. Hilt, C.A. Gallegos, C.A. Gordon, M.A.  
1060 Giedlin, G. Mullenbach, and P. Tekamp-Olson. 1995. IL-8 induces neutrophil  
1061 chemotaxis predominantly via type I IL-8 receptors. *J. Immunol.*
- 1062 Van Handel, B., S.L. Prashad, N. Hassanzadeh-Kiabi, A. Huang, M. Magnusson, B.  
1063 Atanassova, A. Chen, E.I. Hamalainen, and H.K.A. Mikkola. 2010. The first trimester  
1064 human placenta is a site for terminal maturation of primitive erythroid cells. *Blood*.  
1065 doi:10.1182/blood-2010-04-279489.
- 1066 Huhn, O., M.A. Ivarsson, L. Gardner, M. Hollinshead, J.C. Stinchcombe, P. Chen, N.  
1067 Shreeve, O. Chazara, L.E. Farrell, J. Theorell, H. Ghadially, P. Parham, G. Griffiths, A.  
1068 Horowitz, A. Moffett, A.M. Sharkey, and F. Colucci. 2020. Distinctive phenotypes and  
1069 functions of innate lymphoid cells in human decidua during early pregnancy. *Nat.*  
1070 *Commun.* doi:10.1038/s41467-019-14123-z.
- 1071 Ingman, K., V.J.K.W. Cookson, C.J.P. Jones, and J.D. Aplin. 2010. Characterisation of  
1072 Hofbauer Cells in First and Second Trimester Placenta: Incidence, Phenotype, Survival  
1073 in vitro and Motility. *Placenta*. doi:10.1016/j.placenta.2010.03.003.
- 1074 Johnson, E.L., and R. Chakraborty. 2012. Placental Hofbauer cells limit HIV-1 replication  
1075 and potentially offset mother to child transmission (MTCT) by induction of  
1076 immunoregulatory cytokines. *Retrovirology*. doi:10.1186/1742-4690-9-101.
- 1077 Johnson, G.A., R.C. Burghardt, F.W. Bazer, and T.E. Spencer. 2003. Osteopontin: Roles in  
1078 Implantation and Placentation1. *Biol. Reprod.* doi:10.1095/biolreprod.103.020651.
- 1079 Kawasaki, T., and T. Kawai. 2014. Toll-like receptor signaling pathways. *Front. Immunol.*  
1080 doi:10.3389/fimmu.2014.00461.
- 1081 Kobayashi, N., P. Karisola, V. Peña-Cruz, D.M. Dorfman, M. Jinushi, S.E. Umetsu, M.J.  
1082 Butte, H. Nagumo, I. Chernova, B. Zhu, A.H. Sharpe, S. Ito, G. Dranoff, G.G. Kaplan,  
1083 J.M. Casasnovas, D.T. Umetsu, R.H. Dekruff, and G.J. Freeman. 2007. T cell  
1084 Immunoglobulin Mucin Protein (TIM)-4 binds phosphatidylserine and mediates uptake  
1085 of apoptotic cells. *Immunity*. doi:10.1016/j.immuni.2007.11.011.
- 1086 Lien, M.Y., H.C. Tsai, A.C. Chang, M.H. Tsai, C.H. Hua, S.W. Wang, and C.H. Tang. 2018.  
1087 Chemokine CCL4 induces vascular endothelial growth factor C expression and  
1088 lymphangiogenesis by miR-195-3p in oral squamous cell carcinoma. *Front. Immunol.*  
1089 doi:10.3389/fimmu.2018.00412.

- 1090 Loegl, J., U. Hiden, E. Nussbaumer, C. Schlieffsteiner, S. Cvitic, I. Lang, C. Wadsack, B.  
1091 Huppertz, and G. Desoye. 2016. Hofbauer cells of M2a, M2b and M2c polarization may  
1092 regulate fetoplacental angiogenesis. *Reproduction*. doi:10.1530/REP-16-0159.
- 1093 Luizon, M.R., A.C.T. Palei, V.C. Sandrim, L.M. Amaral, J.S.R. Machado, R. Lacchini, R.C.  
1094 Cavalli, G. Duarte, and J.E. Tanus-Santos. 2014. Tissue inhibitor of matrix  
1095 metalloproteinase-1 polymorphism, plasma TIMP-1 levels, and antihypertensive therapy  
1096 responsiveness in hypertensive disorders of pregnancy. *Pharmacogenomics J*.  
1097 doi:10.1038/tpj.2014.26.
- 1098 La Manno, G., R. Soldatov, A. Zeisel, E. Braun, H. Hochgerner, V. Petukhov, K.  
1099 Lidschreiber, M.E. Kastrioti, P. Lönnerberg, A. Furlan, J. Fan, L.E. Borm, Z. Liu, D. van  
1100 Bruggen, J. Guo, X. He, R. Barker, E. Sundström, G. Castelo-Branco, P. Cramer, I.  
1101 Adameyko, S. Linnarsson, and P. V. Kharchenko. 2018. RNA velocity of single cells.  
1102 *Nature*. doi:10.1038/s41586-018-0414-6.
- 1103 Marschallinger, J., T. Iram, M. Zardeneta, S.E. Lee, B. Lehallier, M.S. Haney, J. V.  
1104 Pluvinage, V. Mathur, O. Hahn, D.W. Morgens, J. Kim, J. Tevini, T.K. Felder, H.  
1105 Wolinski, C.R. Bertozzi, M.C. Bassik, L. Aigner, and T. Wyss-Coray. 2020. Lipid-  
1106 droplet-accumulating microglia represent a dysfunctional and proinflammatory state in  
1107 the aging brain. *Nat. Neurosci*. doi:10.1038/s41593-019-0566-1.
- 1108 McGovern, N., A. Shin, G. Low, D. Low, K. Duan, L.J. Yao, R. Msallam, I. Low, N.B.  
1109 Shadan, H.R. Sumatoh, E. Soon, J. Lum, E. Mok, S. Hubert, P. See, E.H. Kunxiang,  
1110 Y.H. Lee, B. Janela, M. Choolani, C.N.Z. Mattar, Y. Fan, T.K.H. Lim, D.K.H. Chan,  
1111 K.K. Tan, J.K.C. Tam, C. Schuster, A. Elbe-Bürger, X.N. Wang, V. Bigley, M. Collin,  
1112 M. Haniffa, A. Schlitzer, M. Poidinger, S. Albani, A. Larbi, E.W. Newell, J.K.Y. Chan,  
1113 and F. Ginhoux. 2017. Human fetal dendritic cells promote prenatal T-cell immune  
1114 suppression through arginase-2. *Nature*. 546:662–666. doi:10.1038/nature22795.
- 1115 Pavlov, O. V., A. V. Selutin, O.M. Pavlova, and S.A. Selkov. 2020. Two patterns of cytokine  
1116 production by placental macrophages. *Placenta*. doi:10.1016/j.placenta.2020.01.005.
- 1117 Pierleoni, C., M. Castellucci, P. Kaufmann, L.R. Lund, and B.S. Nielsen. 2003. Urokinase  
1118 receptor is up-regulated in endothelial cells and macrophages associated with fibrinoid  
1119 deposits in the human placenta. *Placenta*. doi:10.1016/S0143-4004(03)00082-1.
- 1120 Plaks, V., J. Rinkenberger, J. Dai, M. Flannery, M. Sund, K. Kanasaki, W. Ni, R. Kalluri, and  
1121 Z. Werb. 2013. Matrix metalloproteinase-9 deficiency phenocopies features of  
1122 preeclampsia and intrauterine growth restriction. *Proc. Natl. Acad. Sci. U. S. A*.  
1123 doi:10.1073/pnas.1309561110.
- 1124 Poggio, P., J.B. Grau, B.C. Field, R. Sainger, W.F. Seefried, F. Rizzolio, and G. Ferrari.  
1125 2011. Osteopontin controls endothelial cell migration in vitro and in excised human  
1126 valvular tissue from patients with calcific aortic stenosis and controls. *J. Cell. Physiol*.  
1127 doi:10.1002/jcp.22549.

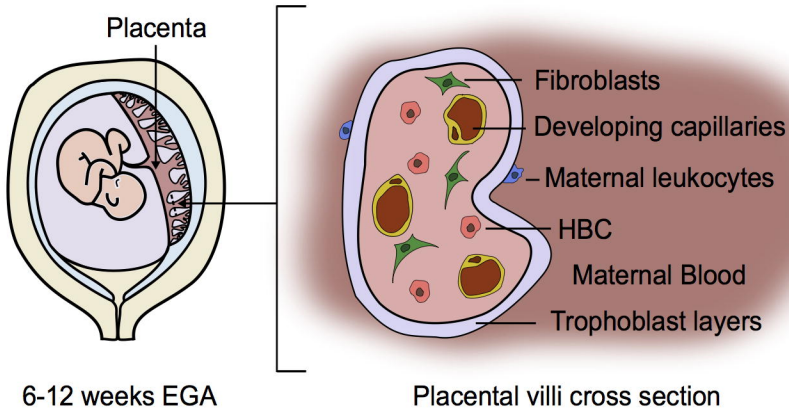
- 1128 Rackaityte, E., J. Halkias, E.M. Fukui, V.F. Mendoza, C. Hayzelden, E.D. Crawford, K.E.  
1129 Fujimura, T.D. Burt, and S. V. Lynch. 2020. Viable bacterial colonization is highly  
1130 limited in the human intestine in utero. *Nat. Med.* doi:10.1038/s41591-020-0761-3.
- 1131 Ramachandran, P., R. Dobie, J.R. Wilson-Kanamori, E.F. Dora, B.E.P. Henderson, N.T. Luu,  
1132 J.R. Portman, K.P. Matchett, M. Brice, J.A. Marwick, R.S. Taylor, M. Efremova, R.  
1133 Vento-Tormo, N.O. Carragher, T.J. Kendall, J.A. Fallowfield, E.M. Harrison, D.J. Mole,  
1134 S.J. Wigmore, P.N. Newsome, C.J. Weston, J.P. Iredale, F. Tacke, J.W. Pollard, C.P.  
1135 Ponting, J.C. Marioni, S.A. Teichmann, and N.C. Henderson. 2019. Resolving the  
1136 fibrotic niche of human liver cirrhosis at single-cell level. *Nature.* doi:10.1038/s41586-  
1137 019-1631-3.
- 1138 Reyes, L., and T.G. Golos. 2018. Hofbauer cells: Their role in healthy and complicated  
1139 pregnancy. *Front. Immunol.* doi:10.3389/fimmu.2018.02628.
- 1140 Salcedo, R., M.L. Ponce, H.A. Young, K. Wasserman, J.M. Ward, H.K. Kleinman, J.J.  
1141 Oppenheim, and W.J. Murphy. 2000. Human endothelial cells express CCR2 and  
1142 respond to MCP-1: Direct role of MCP-1 in angiogenesis and tumor progression. *Blood.*  
1143 doi:10.1182/blood.v96.1.34.013a49\_34\_40.
- 1144 Savina, A., C. Jancic, S. Hugues, P. Guernonprez, P. Vargas, I.C. Moura, A.M. Lennon-  
1145 Duménil, M.C. Seabra, G. Raposo, and S. Amigorena. 2006. NOX2 Controls  
1146 Phagosomal pH to Regulate Antigen Processing during Crosspresentation by Dendritic  
1147 Cells. *Cell.* doi:10.1016/j.cell.2006.05.035.
- 1148 Schliefssteiner, C., M. Peinhaupt, S. Kopp, J. Lögl, I. Lang-Olip, U. Hiden, A. Heinemann, G.  
1149 Desoye, and C. Wadsack. 2017. Human placental Hofbauer cells maintain an anti-  
1150 inflammatory M2 phenotype despite the presence of gestational diabetes mellitus. *Front.*  
1151 *Immunol.* doi:10.3389/fimmu.2017.00888.
- 1152 Sedlyarov, V., R. Eichner, E. Girardi, P. Essletzbichler, U. Goldmann, P. Nunes-Hasler, I.  
1153 Srdic, A. Moskovskich, L.X. Heinz, F. Kartnig, J.W. Bigenzahn, M. Rebsamen, P.  
1154 Kovarik, N. Demaurex, and G. Superti-Furga. 2018. The Bicarbonate Transporter  
1155 SLC4A7 Plays a Key Role in Macrophage Phagosome Acidification. *Cell Host Microbe.*  
1156 doi:10.1016/j.chom.2018.04.013.
- 1157 Sharkey, A.M., A. King, D.E. Clark, T.D. Burrows, P.P. Jokhi, D.S. Charnock-Jones, Y.W.  
1158 Loke, and S.K. Smith. 1999. Localization of Leukemia Inhibitory Factor and Its  
1159 Receptor in Human Placenta Throughout Pregnancy<sup>1</sup>. *Biol. Reprod.*  
1160 doi:10.1095/biolreprod60.2.355.
- 1161 Shi, J., and P.K. Wei. 2016. Interleukin-8: A potent promoter of angiogenesis in gastric  
1162 cancer. *Oncol. Lett.* doi:10.3892/ol.2015.4035.
- 1163 Solders, M., L. Gorchs, E. Tiblad, S. Gidlöf, E. Leeansyah, J. Dias, J.K. Sandberg, I.  
1164 Magalhaes, A.C. Lundell, and H. Kaipe. 2019. Recruitment of MAIT cells to the  
1165 intervillous space of the placenta by placenta-derived chemokines. *Front. Immunol.*

- 1166 doi:10.3389/fimmu.2019.01300.
- 1167 Stamatovic, S.M., R.F. Keep, M. Mostarica-Stojkovic, and A. V. Andjelkovic. 2006. CCL2  
1168 Regulates Angiogenesis via Activation of Ets-1 Transcription Factor. *J. Immunol.*  
1169 doi:10.4049/jimmunol.177.4.2651.
- 1170 Stewart, B.J., J.R. Ferdinand, M.D. Young, T.J. Mitchell, K.W. Loudon, A.M. Riding, N.  
1171 Richoz, G.L. Frazer, J.U.L. Staniforth, F.A.V. Braga, R.A. Botting, D.M. Popescu, R.  
1172 Vento-Tormo, E. Stephenson, A. Cagan, S.J. Farndon, K. Polanski, M. Efremova, K.  
1173 Green, M.D.C. Velasco-Herrera, C. Guzzo, G. Collord, L. Mamanova, T. Aho, J.N.  
1174 Armitage, A.C.P. Riddick, I. Mushtaq, S. Farrell, D. Rampling, J. Nicholson, A. Filby, J.  
1175 Burge, S. Lisgo, S. Lindsay, M. Bajenoff, A.Y. Warren, G.D. Stewart, N. Sebire, N.  
1176 Coleman, M. Haniffa, S.A. Teichmann, S. Behjati, and M.R. Clatworthy. 2019.  
1177 Spatiotemporal immune zonation of the human kidney. *Science (80-. )*.  
1178 doi:10.1126/science.aat5031.
- 1179 Street, K., D. Risso, R.B. Fletcher, D. Das, J. Ngai, N. Yosef, E. Purdom, and S. Dudoit.  
1180 2018. Slingshot: Cell lineage and pseudotime inference for single-cell transcriptomics.  
1181 *BMC Genomics*. doi:10.1186/s12864-018-4772-0.
- 1182 Sutton, L., D.Y. Mason, and C.W. Redman. 1983. HLA-DR positive cells in the human  
1183 placenta. *Immunology*.
- 1184 Swieboda, D., E.L. Johnson, J. Beaver, L. Haddad, E.A.L. Enninga, M. Hathcock, S. Cordes,  
1185 V. Jean, I. Lane, I. Skountzou, and R. Chakraborty. 2020. Baby's First Macrophage:  
1186 Temporal Regulation of Hofbauer Cell Phenotype Influences Ligand-Mediated Innate  
1187 Immune Responses across Gestation. *J. Immunol.* doi:10.4049/jimmunol.1901185.
- 1188 Tang, Z., V.M. Abrahams, G. Mor, and S. Guller. 2011. Placental Hofbauer cells and  
1189 complications of pregnancy. *Ann. N. Y. Acad. Sci.* doi:10.1111/j.1749-  
1190 6632.2010.05932.x.
- 1191 Tsang, J.C.H., J.S.L. Vong, L. Ji, L.C.Y. Poon, P. Jiang, K.O. Lui, Y.B. Ni, K.F. To, Y.K.Y.  
1192 Cheng, R.W.K. Chiu, and Y.M.D. Lo. 2017. Integrative single-cell and cell-free plasma  
1193 RNA transcriptomics elucidates placental cellular dynamics. *Proc. Natl. Acad. Sci. U. S.*  
1194 *A.* doi:10.1073/pnas.1710470114.
- 1195 Turco, M.Y., and A. Moffett. 2019. Development of the human placenta. *Dev.*  
1196 doi:10.1242/dev.163428.
- 1197 Vento-Tormo, R., M. Efremova, R.A. Botting, M.Y. Turco, M. Vento-Tormo, K.B. Meyer,  
1198 J.E. Park, E. Stephenson, K. Polański, A. Goncalves, L. Gardner, S. Holmqvist, J.  
1199 Henriksson, A. Zou, A.M. Sharkey, B. Millar, B. Innes, L. Wood, A. Wilbrey-Clark,  
1200 R.P. Payne, M.A. Ivarsson, S. Lisgo, A. Filby, D.H. Rowitch, J.N. Bulmer, G.J. Wright,  
1201 M.J.T. Stubbington, M. Haniffa, A. Moffett, and S.A. Teichmann. 2018. Single-cell  
1202 reconstruction of the early maternal–fetal interface in humans. *Nature*.  
1203 doi:10.1038/s41586-018-0698-6.

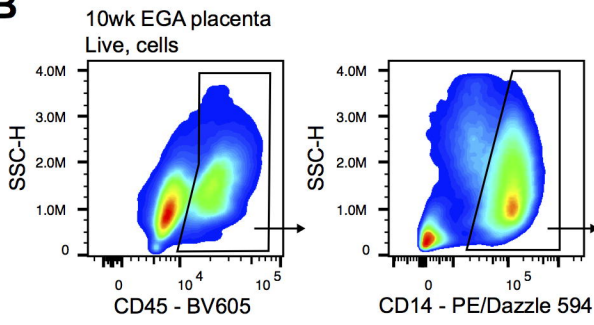
- 1204 Wang, X.N., N. McGovern, M. Gunawan, C. Richardson, M. Windebank, T.W. Siah, H.Y.  
1205 Lim, K. Fink, J.L.Y. Li, L.G. Ng, F. Ginhoux, V. Angeli, M. Collin, and M. Haniffa.  
1206 2014. A three-dimensional atlas of human dermal leukocytes, lymphatics, and blood  
1207 vessels. *J. Invest. Dermatol.* 134:965–974. doi:10.1038/jid.2013.481.
- 1208 Ward, M.G., G. Li, and M. Hao. 2018. Apoptotic  $\beta$ -cells induce macrophage reprogramming  
1209 under diabetic conditions. *J. Biol. Chem.* doi:10.1074/jbc.RA118.004565.
- 1210 Wu, Y., Y.-Y. Li, K. Matsushima, T. Baba, and N. Mukaida. 2008. CCL3-CCR5 Axis  
1211 Regulates Intratumoral Accumulation of Leukocytes and Fibroblasts and Promotes  
1212 Angiogenesis in Murine Lung Metastasis Process. *J. Immunol.*  
1213 doi:10.4049/jimmunol.181.9.6384.
- 1214 Young, O.M., Z. Tang, T. Niven-Fairchild, S. Tadesse, G. Krikun, E.R. Norwitz, G. Mor,  
1215 V.M. Abrahams, and S. Guller. 2015. Toll-like Receptor-Mediated Responses by  
1216 Placental Hofbauer Cells (HBCs): A Potential Pro-Inflammatory Role for Fetal M2  
1217 Macrophages. *Am. J. Reprod. Immunol.* doi:10.1111/aji.12336.
- 1218 Zeng, Y., J. He, Z. Bai, Z. Li, Y. Gong, C. Liu, Y. Ni, J. Du, C. Ma, L. Bian, Y. Lan, and B.  
1219 Liu. 2019. Tracing the first hematopoietic stem cell generation in human embryo by  
1220 single-cell RNA sequencing. *Cell Res.* doi:10.1038/s41422-019-0228-6.
- 1221



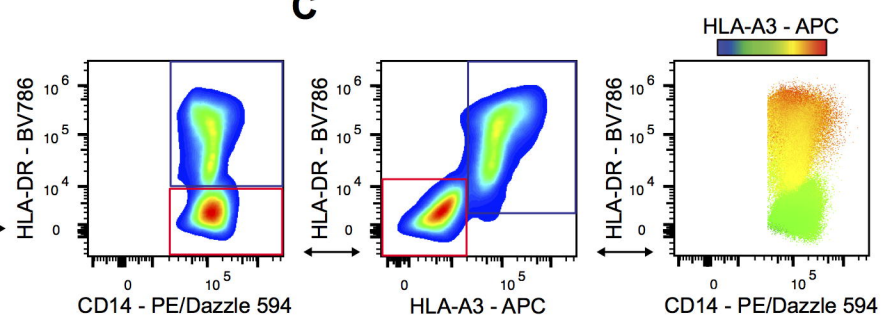
**A**



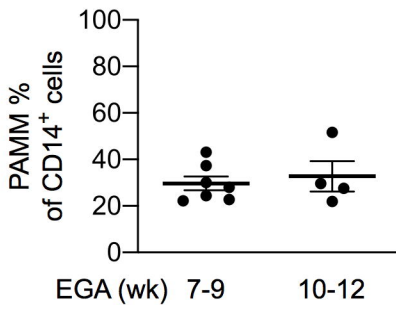
**B**



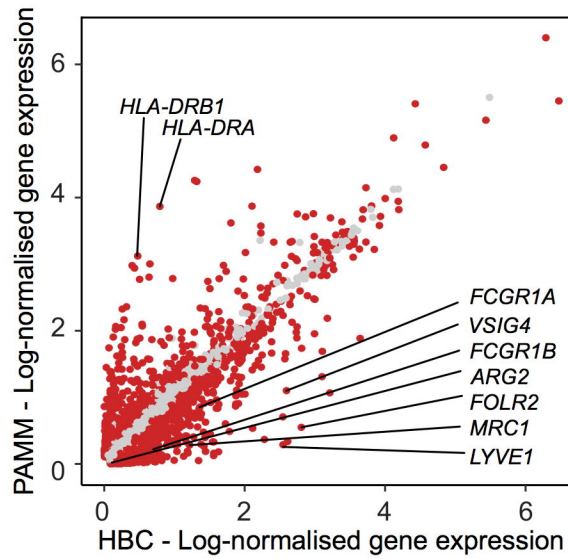
**C**



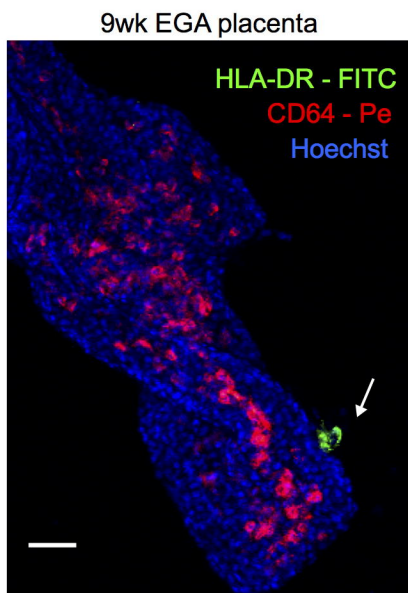
**D**



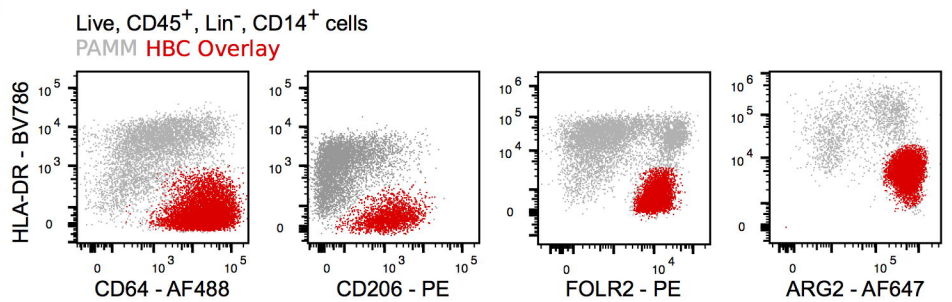
**F**

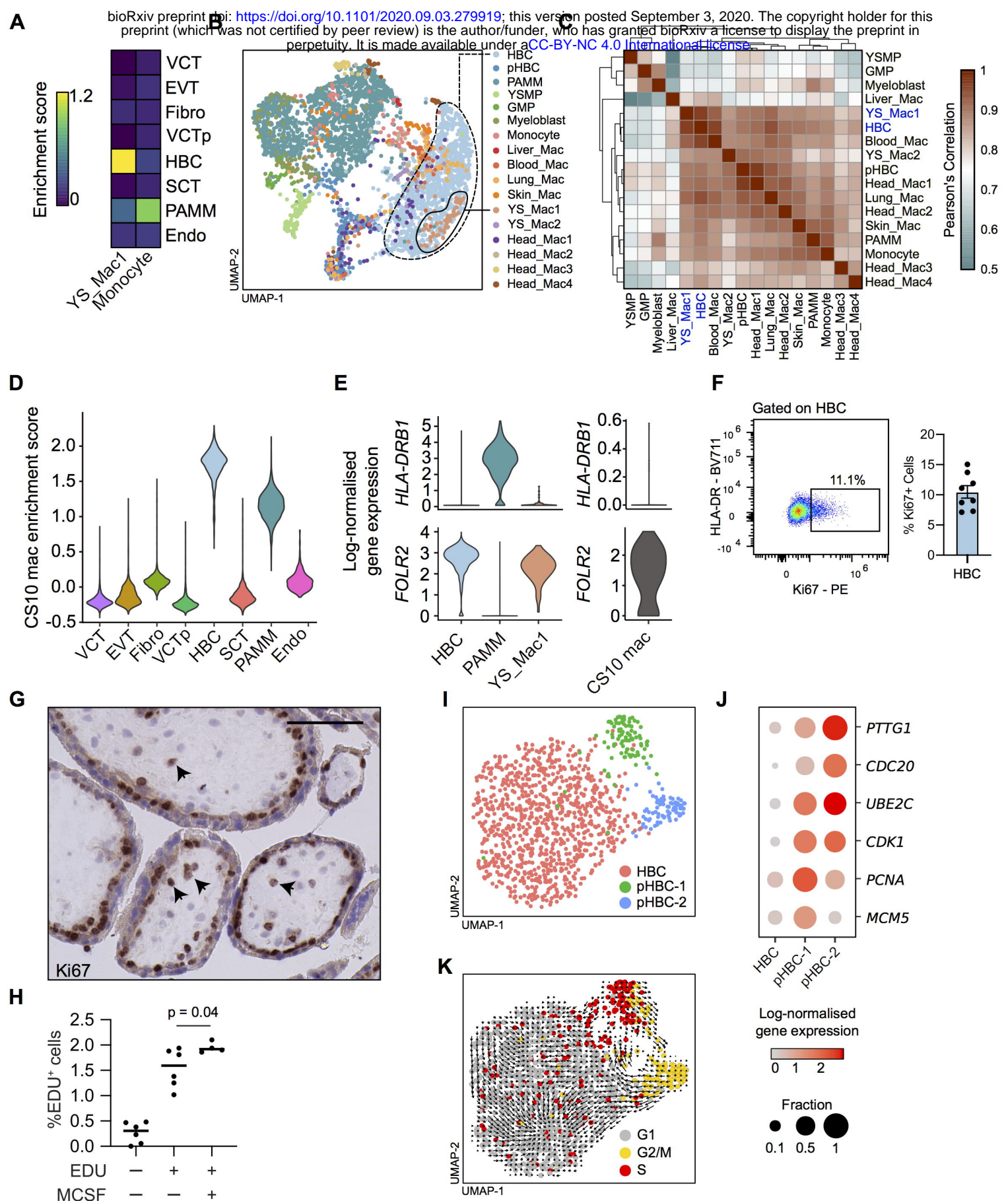


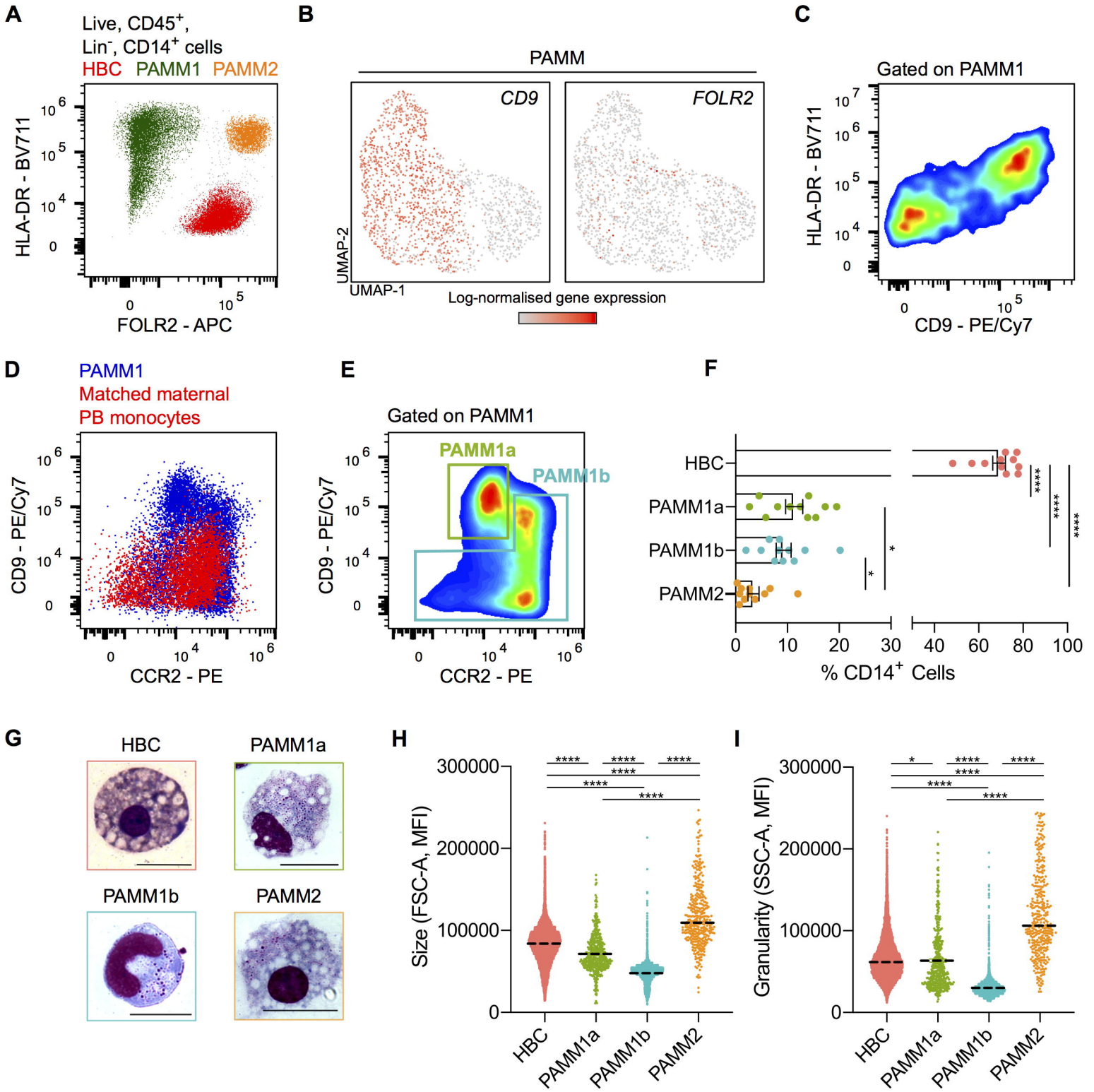
**E**

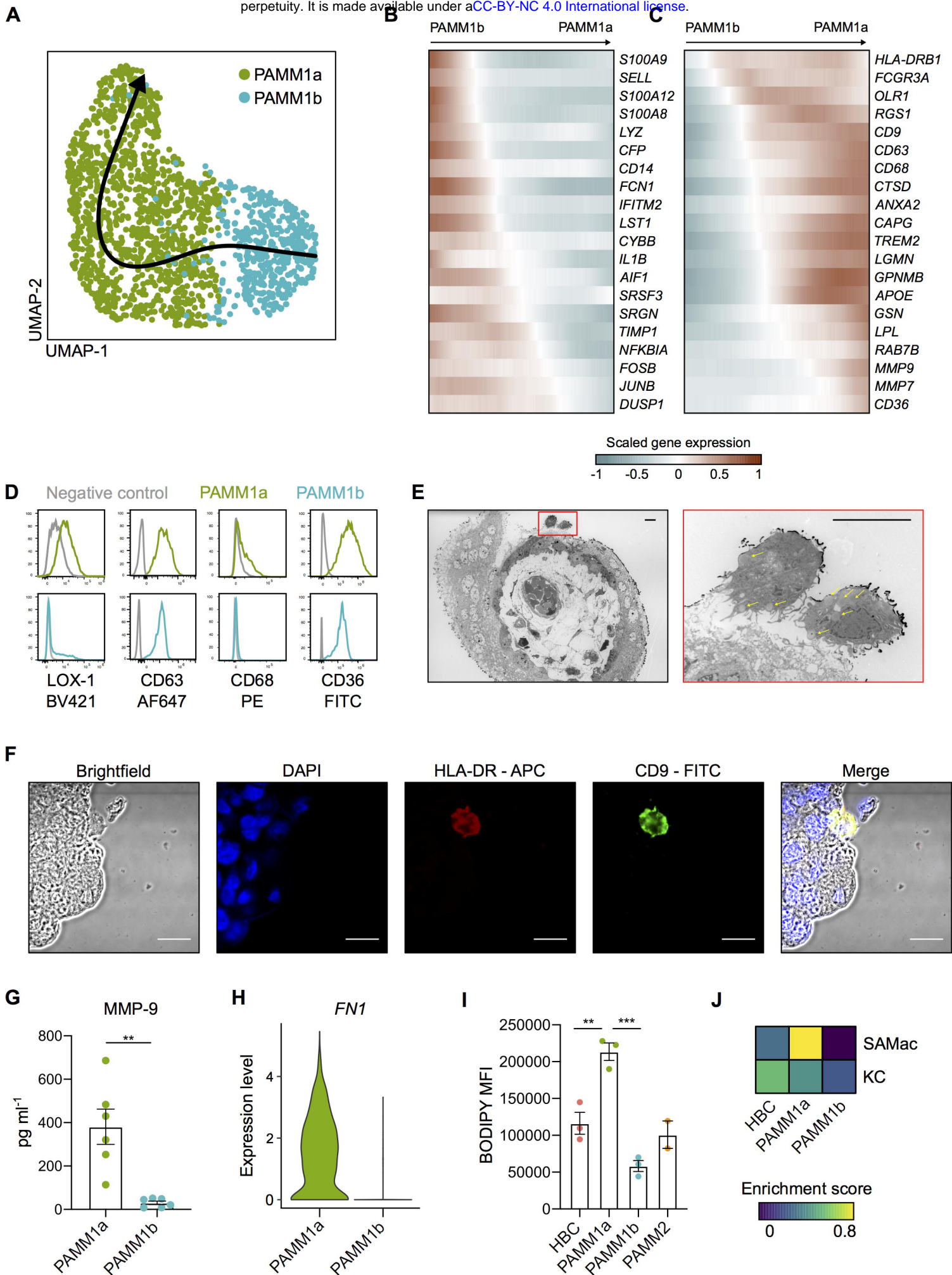


**G**

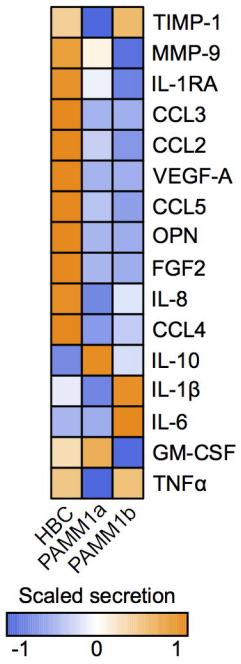




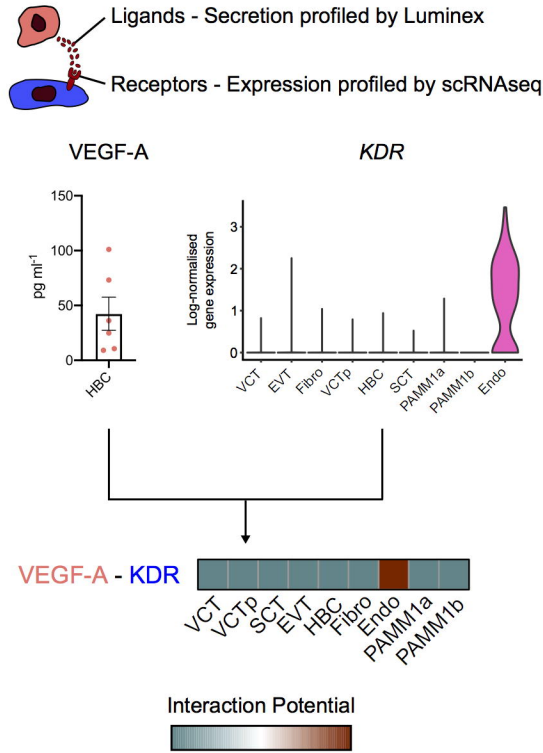




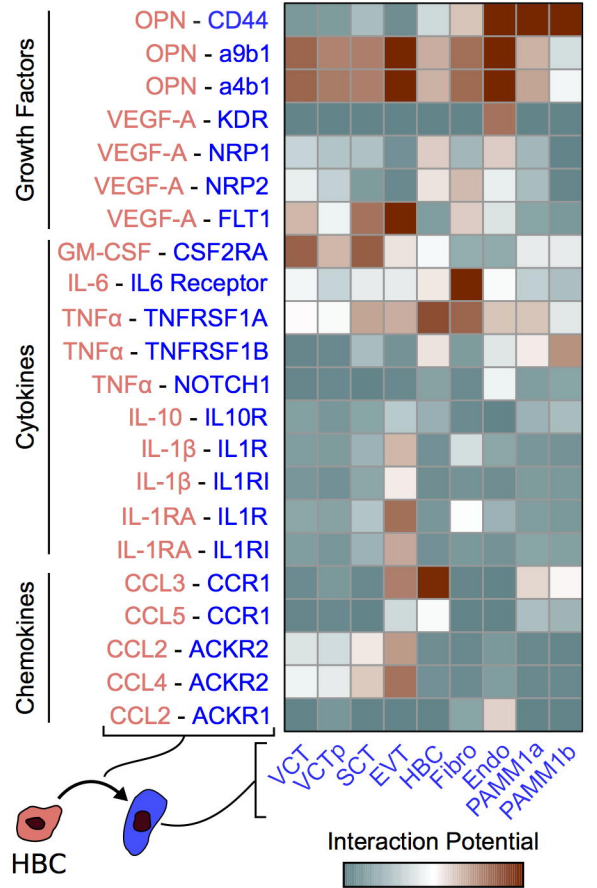
**A**



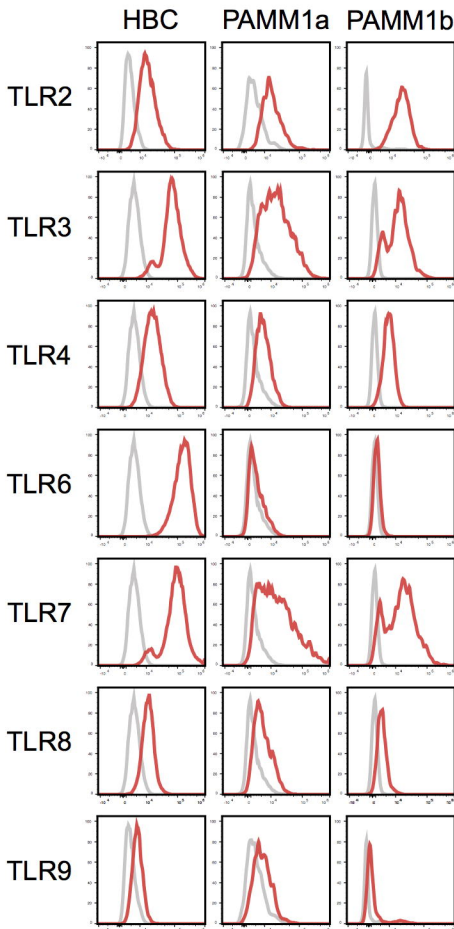
**B**



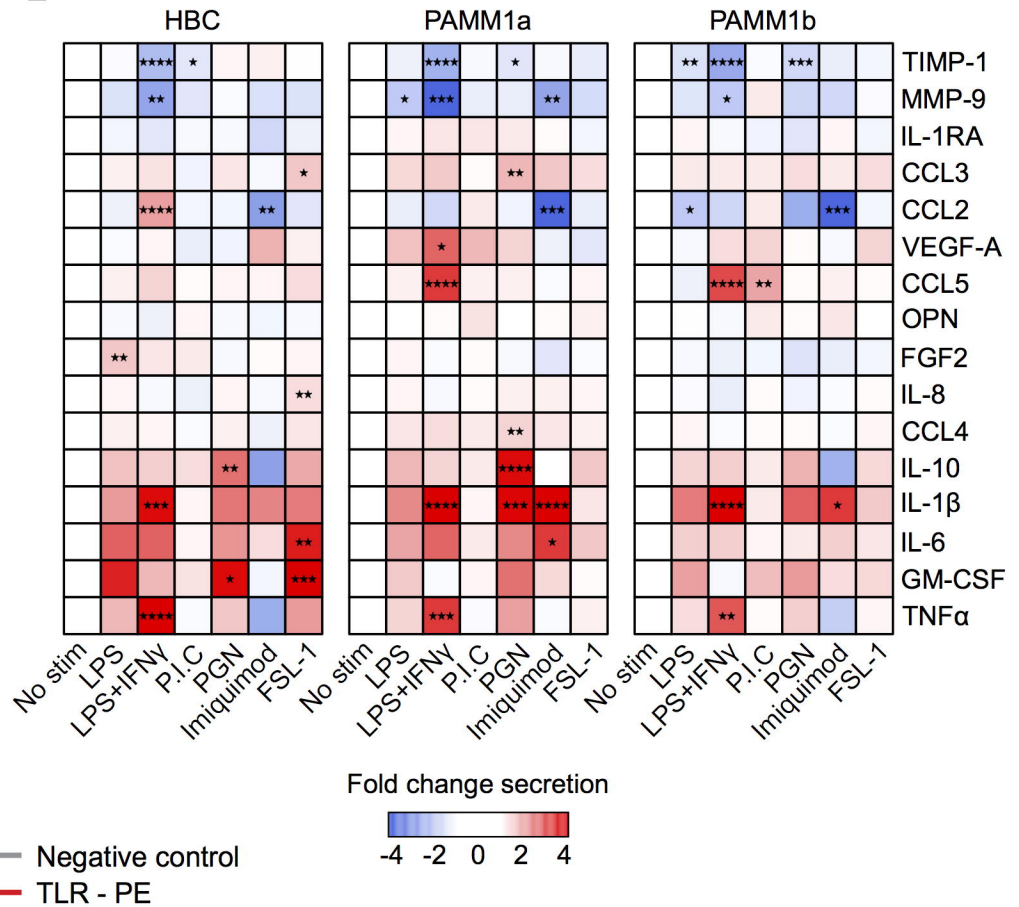
**C**



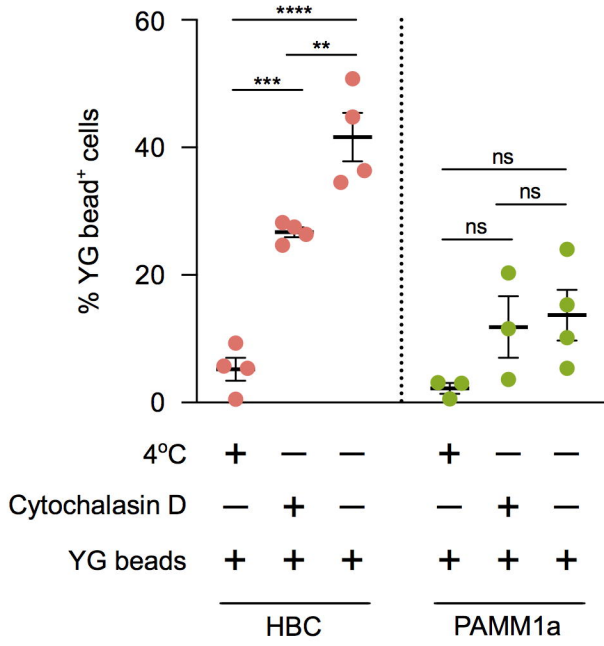
**D**



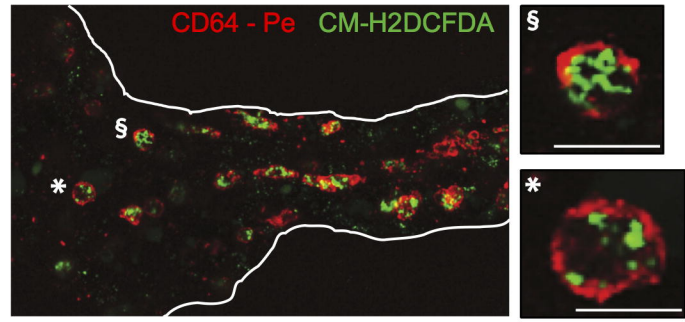
**E**



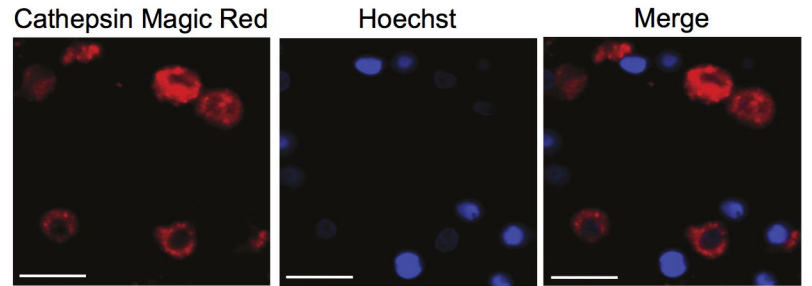
**A**



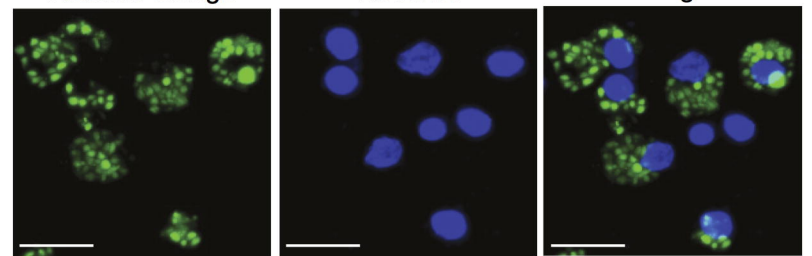
**B**



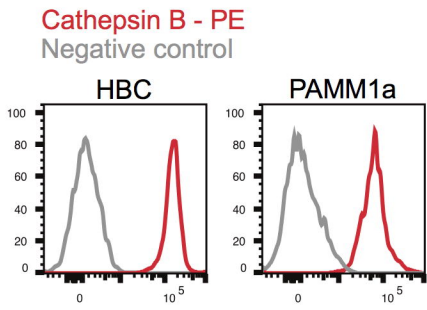
**D**



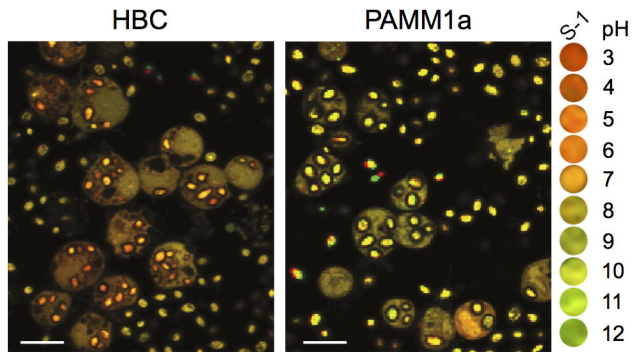
**E**



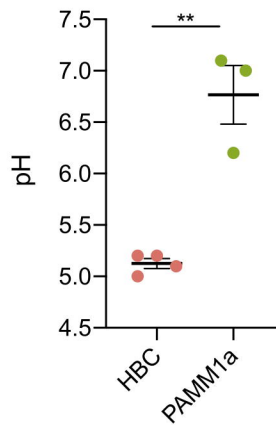
**C**



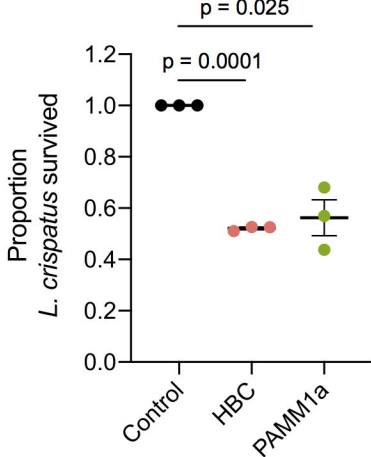
**F**



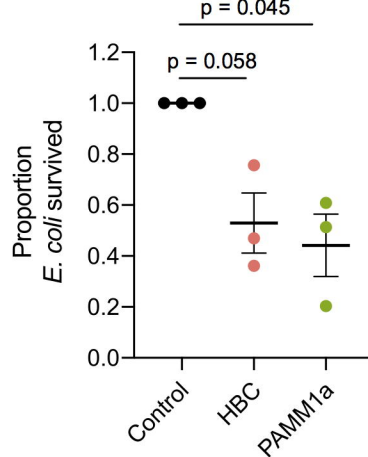
**G**



**H**



**I**



**J**

